arXiv:2509.07031v1 [stat.ME] 7 Sep 2025

Scalable Sample-to-Population Estimation of Hyperbolic Space Models for Hypergraphs

Cornelius Fritz* Yubai Yuan*

Michael Schweinberger

Abstract

Hypergraphs are useful mathematical representations of overlapping and nested subsets of interacting units, including groups of genes or brain regions, economic cartels, political or military coalitions, and groups of products that are purchased together. Despite the vast range of applications, the statistical analysis of hypergraphs is challenging: There are many hyperedges of small and large sizes, and hyperedges can overlap or be nested. We develop a novel statistical approach to hypergraphs with overlapping and nested hyperedges of varying sizes and levels of sparsity, which is amenable to scalable sample-to-population estimation with non-asymptotic theoretical guarantees. First, we introduce a probabilistic framework that embeds the units of a hypergraph in an unobserved hyperbolic space capturing core-periphery structure along with local structure in hypergraphs. Second, we develop scalable manifold optimization algorithms for learning hyperbolic space models based on samples from a hypergraph. Third, we show that the positions of units are identifiable (up to rotations) and provide non-asymptotic theoretical guarantees based on samples from a hypergraph. We use the framework to detect core-periphery structure along with proximity among U.S. politicians based on historical media reports.

*The first two authors are joint first authors and are listed in alphabetical order.

Keywords: Hypergraph Sampling, Latent Space Model, Manifold Learning

1 Introduction

Hypergraphs are useful mathematical representations of overlapping and nested subsets of interacting units, including groups of genes or brain regions, which cooperate in order to perform vital biological functions; economic cartels of companies that collude with an eye to reducing competition and inflating the prices of goods and services; political or military coalitions of state or non-state actors seeking to achieve shared political or military goals; and groups of products that are purchased together. An example of a hypergraph is shown in Figure 1. The displayed hypergraph with five units is a subset of a hypergraph with 678 units we analyze in Section 7.

Despite the vast range of applications, the statistical analysis of hypergraphs is challenging, for at least three reasons. First, a hypergraph with N units consists of $\sum_{k=2}^{N} \binom{N}{k} = 2^N - N - 1$ possible hyperedges. In other words, the number of possible hyperedges is exponential in N, whereas the number of possible edges in a graph is quadratic in N. As a result, the statistical analysis of hypergraphs is more challenging than the statistical analysis of graphs. These challenges are exacerbated by recent advances in collecting digital data, which have enabled the collection of large hypergraphs (Kim et al., 2023; Maleki et al., 2022). Second, hyperedges can overlap, and the probabilities of overlapping hyperedges should be related: e.g., the probabilities of publications involving researchers 1, 2, and 3 (hyperedge $\{1, 2, 3\}$) and researchers 1, 2, and 4 (hyperedge $\{1, 2, 4\}$) should be related, because both publications involve researchers 1 and 2. Third, small hyperedges can be nested in large hyperedges, and the probabilities of nested hyperedges should be related: e.g., if researchers 1 and 2 publish with researchers 3 (hyperedge $\{1, 2, 3\}$) and 4 (hyperedge $\{1, 2, 4\}$), then 1 and 2 may very well publish with both 3 and 4 (hyperedge $\{1, 2, 3, 4\}$).

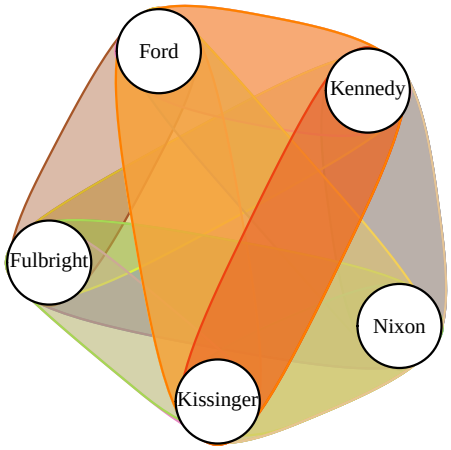

Figure 1: A hypergraph with five U.S. politicians, where hyperedges represent subsets of politicians mentioned together in U.S. Newswire articles between 1900 and 1977. There are ten hyperedges of size two, five hyperedges of size three, and one hyperedge of size four, which are represented by colored contours.

Existing approaches to hypergraphs include hyperedge incidence models (Yu and Zhu, 2025), random geometric hypergraphs with positions in Euclidean space (Turnbull et al., 2023), stochastic block models (Ng and Murphy, 2022; Yuan et al., 2022; Brusa and Matias, 2024a), tensor-based models (Lyu et al., 2023; Ghoshdastidar and Dukkipati, 2014; Yuan and Qu, 2023), and hypergraph neural networks (Kim et al., 2024), among other models (e.g., Nandy and Bhattacharya, 2024). These approaches tackle some of the mentioned challenges, but not all of them: e.g., many existing approaches can be applied to small hypergraphs, but cannot be applied to large hypergraphs owing to the computing time required to learn from them (e.g., Turnbull et al., 2023; Ng and Murphy, 2022; Brusa and Matias, 2024a). Those approaches that are scalable achieve scalability at the expense of model realism: e.g., some approaches restrict attention to hyperedges of a fixed size (e.g., Lyu et al., 2023; Ghoshdastidar and Dukkipati, 2014), which neglects hyperedges of all other sizes and ignores the fact that small hyperedges are nested into large hyperedges. Other approaches assume that realized hyperedges of all sizes are independent and iden-

tically distributed draws from a common probability law (e.g., Yu and Zhu, 2025), which specifies a model for realized hyperedges but does not provide an explicit model for unrealized hyperedges. In addition, the assumption that the same probability law generates hyperedges of different sizes may not be satisfied in real-world applications. For example, the data used in Section 7 indicate that larger hyperedges exhibit higher levels of sparsity: e.g., the proportions of realized hyperedges of sizes 2, 3, 4, 5, and 6 are 2×10^{-2}, 5×10^{-5}, 1×10^{-7}, 5×10^{-10}, and 2×10^{-12}, respectively. These observations suggest that hyperedges of different sizes are generated by different probability laws.

Contributions We introduce a statistical framework for hyperedges of varying sizes and levels of sparsity, which addresses all of the above challenges and is amenable to scalable sample-to-population estimation with non-asymptotic theoretical guarantees:

1. We introduce a novel class of hyperbolic space models capturing core-periphery structure along with local structure in hypergraphs in Section 3.

2. We estimate hyperbolic space models based on samples. Sample-to-population estimation is crucial, for two reasons. First, it may not be possible to observe the entire population hypergraph due to data collection constraints. Second, even when the entire population hypergraph is observed, using observations of $2^N - N - 1$ possible hyperedges may be infeasible when N is large. We discuss sampling in Section 4.1 and introduce scalable manifold optimization algorithms for learning hyperbolic space models from samples of hyperedges in Section 4.2. We complement scalable learning methods by scalable simulation methods in Section 4.3.

3. We show in Section 3.2 that the positions of units in hyperbolic space are identifiable (up to rotations) and establish non-asymptotic theoretical guarantees based on a finite number of units N and a finite number of sampled hyperedges in Section 5.

The theoretical results in Section 5 are supported by simulation results in Section 6.

4. We use hyperbolic space models in Section 7 to detect core-periphery structure along with proximity among U.S. politicians based on historical media reports.

To pave the way for hyperbolic space models, we first provide background on hyperbolic space in Section 2.

Notation Let $\mathcal{V} \coloneqq \{1, \ldots, N\}$ be a population with $N \geq 3$ units. We consider hyperedges $e \subseteq \mathcal{V}$ of size $|e| \in \{2, \ldots, K\}$ ($K \in \{3, \ldots, N\}$). Throughout, we assume that K is independent of N. The set of all possible hyperedges of size k is denoted by $\mathcal{E}_k \coloneqq \{e : \ e \subseteq \mathcal{V}, \ |e| = k\}$ $(k = 2, \ldots, K)$ and the set of all hyperedges of all sizes is denoted by $\mathcal{E} \coloneqq \bigcup_{k=2}^{K} \mathcal{E}_k$. Let $Z_e \in \{0, 1\}$ be an indicator of an hyperedge, where $Z_e \coloneqq 1$ if hyperedge e exists and $Z_e \coloneqq 0$ otherwise. The collection of indicators $\boldsymbol{Z}_{\mathcal{E}} = (Z_e)_{e \in \mathcal{E}}$ represents a hypergraph, while $\boldsymbol{Z}_{\mathcal{E}_k} = (Z_e)_{e \in \mathcal{E}_k}$ refers to all hyperedges of size $k \in \{2, \ldots, K\}$. For any vector $\boldsymbol{x} \coloneqq (x_1, \ldots, x_p) \in \mathbb{R}^p$ of dimension $p \geq 1$, the Euclidean norm is defined by $\|\boldsymbol{x}\|_2 \coloneqq (\sum_{i=1}^{p} x_i^2)^{1/2}$. For any matrix $\boldsymbol{A} \in \mathbb{R}^{p \times p}$, the Frobenius norm is denoted by $\|\boldsymbol{A}\|_F \coloneqq (\sum_{i=1}^{p} \sum_{j=1}^{p} A_{i,j}^2)^{1/2}$. We write $a(n) = O(b(n))$ if there exists a finite constant $C > 0$ such that $|a(n) \,/\, b(n)| \leq C$ holds for all large enough n, and $a(n) = O_p(b(n))$ if $|a(n) \,/\, b(n)| \leq C$ holds with a probability tending to 1. We write $a(n) = o(b(n))$ if, for all $\epsilon > 0$, $|a(n) \,/\, b(n)| \ < \epsilon$ holds for all large enough n, and $f(n) \asymp g(n)$ if there exist finite constants $C_1 > 0$ and $C_2 > 0$ such that $C_1 \leq f(n)/g(n) \leq C_2$ holds for all large enough n.

2 Hyperbolic Space

Since many real-world networks exhibit hierarchical structure (Li et al., 2022; Clauset et al., 2008), hyperbolic geometry has grown more popular as a mathematical model of network structure. Hyperbolic space models have been used to model graphs with $\binom{N}{2}$ possible

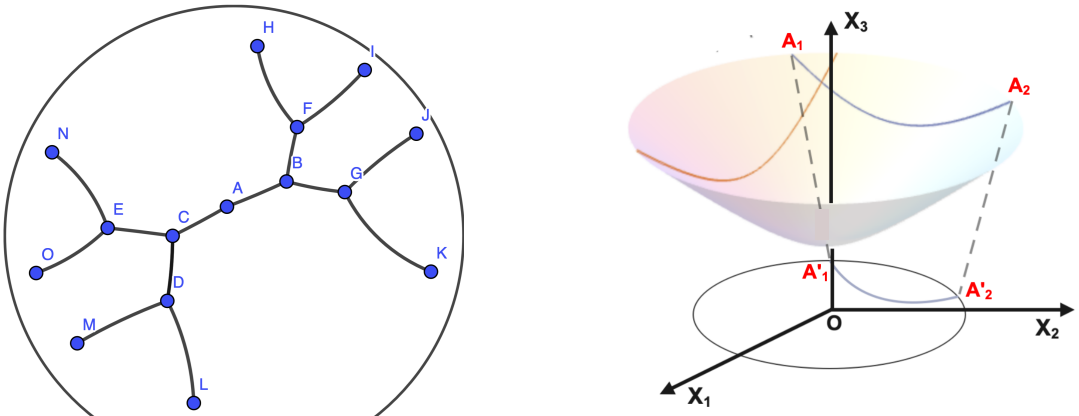

(a) Poincaré disk with tree

(b) Equivalent representations of hyperbolic space

Figure 2: Hyperbolic space: (a) Poincaré disk, including an embedded tree with root A close to the center of the Poincaré disk and leaves H, I, J, K, L, M, N, O close to the boundary of the Poincaré disk. (b) Equivalent representations of hyperbolic space: Poincaré disk and Lorentz model. The segment A_1'–A_2' is the projection of the segment A_1–A_2 in the Lorentz model onto the Poincaré disk.

edges (Krioukov et al., 2010; Smith et al., 2019; Lubold et al., 2023), but not hypergraphs with $2^N - N - 1$ possible hyperedges that can overlap or be nested. To pave the way for hyperbolic space models for hypergraphs, we first provide background on hyperbolic space.

To describe the properties of hyperbolic space, we first introduce two-dimensional hyperbolic space, although we will consider r-dimensional hyperbolic space ($r \geq 2$) throughout the remainder of the manuscript. Hyperbolic space has multiple equivalent representations, including the Poincaré disk, which facilitates interpretation and visualization; and the Lorentz model, which facilitates computing. These two representations of hyperbolic space are visualized in Figure 2.

Poincaré disk The Poincaré disk with radius 1 is defined by

$$\mathcal{P} \;\coloneqq\; \{\boldsymbol{x} \in \mathbb{R}^2 : \|\boldsymbol{x}\|_2 < 1\}.$$

The distance between two points $\boldsymbol{x}_1 \in \mathcal{P}$ and $\boldsymbol{x}_2 \in \mathcal{P}$ on the Poincaré disk is

$$d_{\mathcal{P}}(\boldsymbol{x}_1, \boldsymbol{x}_2) \coloneqq \operatorname{arcosh}\left(1 + \frac{2\,\|\boldsymbol{x}_1 - \boldsymbol{x}_2\|_2^2}{(1 - \|\boldsymbol{x}_1\|_2^2)\,(1 - \|\boldsymbol{x}_2\|_2^2)}\right),$$

where $\operatorname{arcosh}(a) \coloneqq \log(a + \sqrt{a^2 - 1})$ $(a \geq 1)$. A useful property of hyperbolic space is its curvature. The curvature quantifies how much the space deviates from a flat surface (Boumal, 2023): While the curvature of Euclidean space is 0, the curvature of hyperbolic space is negative. The negative curvature of hyperbolic space implies that hyperbolic distance grows as one approaches the boundary of the Poincaré disk. As a result, hyperbolic space can embed trees into a low-dimensional space as demonstrated in Figure 2 (a), helping capture core-periphery structure along with local structure in hypergraphs.

Lorentz model The Lorentz model offers an alternative representation of hyperbolic space and facilitates computing, by providing closed-form representations of geodesics and tangent space (Nickel and Kiela, 2018). The Lorentz model of hyperbolic space is given by

$$\mathcal{L} \;\coloneqq\; \{\boldsymbol{\theta} \in \mathbb{R}^{r+1} : \langle \boldsymbol{\theta}, \boldsymbol{\theta} \rangle_{\mathcal{L}} = -1,\ \theta_1 > 0\},$$

where $\langle \boldsymbol{\theta}, \boldsymbol{\theta} \rangle_{\mathcal{L}} \coloneqq -\theta_1^2 + \sum_{i=2}^{r+1} \theta_i^2$. The associated distance function on $\mathcal{L}$ is

$$d_{\mathcal{L}}(\boldsymbol{\theta}_1, \boldsymbol{\theta}_2) \;\coloneqq\; \operatorname{arcosh}\left(-\langle \boldsymbol{\theta}_1, \boldsymbol{\theta}_2 \rangle_{\mathcal{L}}\right).$$

3 Hyperbolic Space Models for Hypergraphs

We introduce hyperbolic space models for hypergraphs, assuming that the units $1, \ldots, N$ of a hypergraph have positions $\boldsymbol{\theta}_1, \ldots, \boldsymbol{\theta}_N$ in hyperbolic space $\mathcal{L}$.

We assume that the indicators Z_e of hyperedges e are independent Bernoulli($\pi(\alpha_{|e|},\, \boldsymbol{\Theta}_e)$) random variables conditional on sparsity parameters $\alpha_{|e|}$ and positions $\boldsymbol{\Theta}_e \coloneqq (\boldsymbol{\theta}_i)_{i \in e}$ of units involved in hyperedge e:

$$Z_e \mid \alpha_{|e|},\, \boldsymbol{\Theta}_e \;\overset{\text{ind}}{\sim}\; \text{Bernoulli}(\pi(\alpha_{|e|},\, \boldsymbol{\Theta}_e)),$$

where $\pi(\alpha_{|e|}, \boldsymbol{\Theta}_e)$ is the probability of observing hyperedge e. The probability $\pi(\alpha_{|e|}, \boldsymbol{\Theta}_e)$ of observing hyperedge e is of the form

$$\pi(\alpha_{|e|},\, \boldsymbol{\Theta}_e) \;\coloneqq\; \alpha_{|e|}\, \sigma\left(-g(\boldsymbol{\Theta}_e)\right),$$

where

$$\sigma(x) \;\coloneqq\; \frac{2\, \exp(x)}{1 + \exp(x)}, \quad x \in \mathbb{R}.$$

The parameter $\alpha_{|e|} \in (0,\, 1]$ determines the sparsity of hyperedges e of size $|e|$, while the function $g : \boldsymbol{\Theta}_e \mapsto [0,\, \infty)$ captures core-periphery structure along with local structure in hypergraphs. The factor 2 ensures that $\pi(\alpha_{|e|}, \boldsymbol{\Theta}_e) \in (0,\, 1)$.

3.1 Model Specification

To specify the function $g(\boldsymbol{\Theta}_e)$, let

$$d_i^{(e)}(\boldsymbol{\Theta}_e) \;\coloneqq\; \sum_{j \in e \setminus \{i\}} d_{\mathcal{L}}(\boldsymbol{\theta}_i,\, \boldsymbol{\theta}_j)$$

be the sum of distances of unit $i \in e$ to the other units $j \in e \setminus \{i\}$ involved in hyperedge e, and define $g(\boldsymbol{\Theta}_e)$ as the Hölder mean of $d_i^{(e)}(\boldsymbol{\Theta}_e)$ $(i \in e)$:

$$g(\boldsymbol{\Theta}_e) \;\coloneqq\; \left\{ \frac{1}{|e|} \sum_{i \in e} \left[d_i^{(e)}(\boldsymbol{\Theta}_e) \right]^p \right\}^{1/p}. \tag{1}$$

The function $g(\boldsymbol{\Theta}_e)$ approaches $\min_{i \in e}\{d_i^{(e)}(\boldsymbol{\Theta}_e)\}$ as $p \to -\infty$ and $\max_{i \in e}\{d_i^{(e)}(\boldsymbol{\Theta}_e)\}$ as $p \to +\infty$. The advantage of specifying $g(\boldsymbol{\Theta}_e)$ as the Hölder mean of $d_i^{(e)}(\boldsymbol{\Theta}_e)$ $(i \in e)$ is that the Hölder mean is differentiable, in contrast to $\min_{i \in e}\{d_i^{(e)}(\boldsymbol{\Theta}_e)\}$ and $\max_{i \in e}\{d_i^{(e)}(\boldsymbol{\Theta}_e)\}$.

We are interested in large negative values of p, so that $g(\boldsymbol{\Theta}_e)$ is close to $\min_{i \in e}\{d_i^{(e)}(\boldsymbol{\Theta}_e)\}$. Simulation results in Section 7 suggest that conclusions are not sensitive to the value of p as long as $p \leq -20$. In the simulations and application in Sections 6 and 7, we set $p = -20$.

In addition to facilitating computing, the specification of $g(\boldsymbol{\Theta}_e)$ helps capture salient features of hypergraphs:

- **Core-periphery structure.** The close-to-minimum-distance specification of $g(\boldsymbol{\Theta}_e)$ allows hyperedges to emerge from a hierarchical core-periphery structure resembling a tree, whose root is a central unit close to the center of the Poincaré disk and whose leaves are peripheral units close to the boundary of the Poincaré disk, as demonstrated in Figure 2 (a). The close-to-minimum-distance specification is better suited to capturing hierarchical core-periphery structure than the close-to-maximum-distance specification, because the close-to-maximum-distance specification requires all units in an hyperedge to be close to all others, whereas the close-to-minimum-distance specification requires some, but not all units to be close to all others.

- **Pooling strength across overlapping and nested hyperedges.** The function $g(\boldsymbol{\Theta}_e)$ helps pool strength across overlapping and nested hyperedges: e.g., if $e = \{i, j\}$ and $e' = \{i, j, k\}$, the distance $d_{\mathcal{L}}(\boldsymbol{\theta}_i, \boldsymbol{\theta}_j)$ between units i and j is contained in both $g(\boldsymbol{\Theta}_e)$ and $g(\boldsymbol{\Theta}_{e'})$. As a result, the probabilities of hyperedges e and e' are related, and the proposed model is able to leverage information from overlapping and nested hyperedges, helping estimate the distance between i and j.

3.2 Identifiability

The hyperbolic distances among units are determined by the Gram matrix $\boldsymbol{D} \coloneqq \boldsymbol{\Theta}\, \boldsymbol{J}\, \boldsymbol{\Theta}^\top$, where $\boldsymbol{J} \coloneqq \operatorname{diag}(-1, \mathbf{1}_r) \in \mathbb{R}^{(r+1)\times(r+1)}$ and $\mathbf{1}_r \coloneqq (1, \ldots, 1) \in \mathbb{R}^r$, whereas $\boldsymbol{\Theta} \coloneqq (\boldsymbol{\theta}_1^\top, \ldots, \boldsymbol{\theta}_N^\top)^\top$ stores the positions $\boldsymbol{\theta}_1, \ldots, \boldsymbol{\theta}_N \in \mathcal{L}$ of units $1, \ldots, N$. The following propo-

sition establishes the identifiability of Gram matrix $\boldsymbol{D}$ and sparsity parameters $\alpha_2, \ldots, \alpha_K$.

Proposition 1 *The Gram matrix* $\boldsymbol{D} \coloneqq \boldsymbol{\Theta}\,\boldsymbol{J}\,\boldsymbol{\Theta}^\top$ *and the sparsity parameters* $\alpha_2, \ldots, \alpha_K$ *are identifiable provided that* $N > r + 2$.

A proof of Proposition 1 can be found in Supplement A.1. Since $\boldsymbol{D}$ is identifiable, the positions of units can be identified up to a hyperbolic rotation matrix $\boldsymbol{R}$ such that $\boldsymbol{R}\,\boldsymbol{J}\,\boldsymbol{R}^\top = \boldsymbol{J}$. In other words, we can identify an equivalence class of positions, $\{\boldsymbol{\Theta}\,\boldsymbol{R} \mid \boldsymbol{R}\,\boldsymbol{J}\,\boldsymbol{R}^\top = \boldsymbol{J}\}$. The rotation matrix $\boldsymbol{R}$ is the hyperbolic counterpart of the orthogonal transformation on Euclidean space. For example, when $r = 2$, the hyperbolic rotation $\boldsymbol{R}$ is

$$\boldsymbol{R} = \begin{bmatrix} 1 & 0 & 0 \\ 0 & \cos x & -\sin x \\ 0 & \sin x & \cos x \end{bmatrix} \begin{bmatrix} \cosh x & 0 & \sinh x \\ 0 & 1 & 0 \\ \sinh x & 0 & \cosh x \end{bmatrix} \begin{bmatrix} \cosh x & \sinh x & 0 \\ \sinh x & \cosh x & 0 \\ 0 & 0 & 1 \end{bmatrix}.$$

To address the rotation invariance, we perform an eigenvalue decomposition: $\boldsymbol{D} = \boldsymbol{U}\boldsymbol{S}\,\boldsymbol{U}^\top$. Since $\boldsymbol{D}$ has one negative and r positive eigenvalues (Tabaghi and Dokmanić, 2020), $\boldsymbol{S} = \operatorname{diag}(\lambda_1, \ldots, \lambda_{r+1}) \in \mathbb{R}^{(r+1)\times(r+1)}$ is a diagonal matrix with all nonzero eigenvalues of $\boldsymbol{D}$ on the diagonal and $\boldsymbol{U} \in \mathbb{R}^{N\times(r+1)}$ is a matrix of corresponding eigenvectors. The eigenvalues are assumed to have the following order: λ_1 is the negative eigenvalue and $\lambda_2, \ldots, \lambda_{r+1}$ are all positive eigenvalues in decreasing order. Within this equivalence class, we fix positions $\widetilde{\boldsymbol{\Theta}} \coloneqq \boldsymbol{U}|\,\boldsymbol{S}|^{1/2}\boldsymbol{J} \in \{\boldsymbol{\Theta}\,\boldsymbol{R} \mid \boldsymbol{R}\,\boldsymbol{J}\,\boldsymbol{R}^\top = \boldsymbol{J}\}$, where $|\boldsymbol{S}|^{1/2}$ denotes the diagonal matrix whose entries are the square root of the absolute values of the eigenvalues in $\boldsymbol{S}$. Thus, the transformed latent positions $\widetilde{\boldsymbol{\Theta}}$ are identifiable.

4 Sample-to-Population Estimation

Sample-to-population estimation is indispensable, for two reasons. First, it may not be possible to observe the entire population hypergraph. Second, even when the entire population

hypergraph is observed, it may be infeasible to analyze it in its entirety, because it consists of $2^N - N - 1$ possible hyperedges. While reducing the statistical analysis to hyperedges e of size $|e| \leq K$ alleviates the problem, it does not solve it: e.g., in the application in Section 7 with $N = 678$ units, there are more than 1 trillion possible hyperedges of size $|e| \leq 5$ and 8 billion possible hyperedges of size $|e| \leq 4$. A body of data of such size is too large to be analyzed in its entirety, making sample-to-population estimation indispensable.

To pave the way for sample-to-population estimation, we first describe methods for sampling from hypergraphs in Section 4.1. We then introduce scalable statistical methods for learning hyperbolic space models based on samples in Section 4.2, complemented by scalable simulation methods in Section 4.3.

4.1 Sampling from Hypergraphs

To sample from a hypergraph, one can adapt sampling designs for graphs (e.g., Kolaczyk, 2017; Schweinberger et al., 2020, Section 5.2) to hypergraphs. At least two broad classes of sampling designs can be distinguished:

- **Direct sampling** generates a probability sample of hyperedges $e \in \mathcal{E}$, which may be stratified according to the size $|e|$ of hyperedges e and according to whether $Z_e = 0$ (hyperedge e does not exist) or $Z_e = 1$ (hyperedge e exists).

- **Indirect sampling** first generates a probability sample of units $i \in \mathcal{V}$ and then collects data on hyperedges of sampled units, and those connected to them. Examples are ego-centric sampling and link-tracing adapted to hypergraphs.

In the simulations and application in Sections 6 and 7, we sample hyperedges using sample inclusion probabilities

- $\mu_e = n\,|\mathcal{E}_k^{(1)}|/|\mathcal{E}_k^{(0)}|$ for all $e \in \mathcal{E}_k^{(0)}$ with $1 \leq n \leq |\mathcal{E}_k^{(0)}|/|\mathcal{E}_k^{(1)}|$,

- $\mu_e = 1$ for all $e \in \mathcal{E}_k^{(1)}$,

where $\mathcal{E}_k^{(0)} \coloneqq \{e \in \mathcal{E}_k : \ Z_e = 0\}$ is the set of unrealized hyperedges of size k and $\mathcal{E}_k^{(1)} \coloneqq \{e \in \mathcal{E}_k : \ Z_e = 1\}$ is the set of realized hyperedges of size k $(k = 2, \ldots, K)$.

The described sampling design is motivated by the observation that many real-world networks are sparse. As a result, the number of realized hyperedges is small relative to the number of unrealized hyperedges. We therefore sample all realized hyperedges and, for each realized hyperedge, we sample n unrealized hyperedges.

4.2 Learning From Samples

The target of statistical inference is the positions $\boldsymbol{\Theta}$ of units in hyperbolic space along with the sparsity parameters $\alpha_2, \ldots, \alpha_K$, which we denote by $\boldsymbol{\Lambda} \coloneqq (\boldsymbol{\Theta}, \alpha_2, \ldots, \alpha_K)$. To learn $\boldsymbol{\Lambda}$ from data, we first introduce a population loss and then introduce a sample loss.

Population loss If $\mathcal{E}_k^{(0)}$ and $\mathcal{E}_k^{(1)}$ are observed $(k = 2, \ldots, K)$, one can minimize the population loss defined by

$$\ell(\boldsymbol{\Lambda}) \ \coloneqq \ \ell_0(\boldsymbol{\Lambda}) + \ell_1(\boldsymbol{\Lambda}),$$

where

$$\begin{aligned} \ell_0(\boldsymbol{\Lambda}) \ &\coloneqq \ -\sum_{k=2}^{K} \sum_{e \in \mathcal{E}_k^{(0)}} \log(1 - \pi(\alpha_{|e|}, \boldsymbol{\Theta}_e)) \\ \ell_1(\boldsymbol{\Lambda}) \ &\coloneqq \ -\sum_{k=2}^{K} \sum_{e \in \mathcal{E}_k^{(1)}} \log \pi(\alpha_{|e|}, \boldsymbol{\Theta}_e). \end{aligned}$$

Sample loss If samples $\mathcal{S}_k^{(0)}$ and $\mathcal{S}_k^{(1)}$ from $\mathcal{E}_k^{(0)}$ and $\mathcal{E}_k^{(1)}$ $(k = 2, \ldots, K)$ are available, one can approximate the population loss $\ell(\cdot)$ by the sample loss $\widehat{\ell}(\cdot)$ defined by

$$\widehat{\ell}(\boldsymbol{\Lambda}) \ \coloneqq \ \widehat{\ell}_0(\boldsymbol{\Lambda}) + \widehat{\ell}_1(\boldsymbol{\Lambda}),$$

where $\widehat{\ell}_0(\cdot)$ and $\widehat{\ell}_1(\cdot)$ are Horvitz-Thompson estimators of the corresponding population quantities $\ell_0(\cdot)$ and $\ell_1(\cdot)$:

$$\begin{aligned}\widehat{\ell}_0(\boldsymbol{\Lambda}) &\coloneqq -\sum_{k=2}^{K} \sum_{e \in \mathcal{S}_k^{(0)}} \frac{1}{\mu_e} \log(1 - \pi(\alpha_{|e|}, \boldsymbol{\Theta}_e)) \\ \widehat{\ell}_1(\boldsymbol{\Lambda}) &\coloneqq -\sum_{k=2}^{K} \sum_{e \in \mathcal{S}_k^{(1)}} \frac{1}{\mu_e} \log\, \pi(\alpha_{|e|}, \boldsymbol{\Theta}_e).\end{aligned}$$

The weights $\mu_e \in [0, 1]$ are the sample inclusion probabilities of hyperedges $e \in \mathcal{E}$. We consider them known and allow them to depend on Z_e and covariates.

We minimize the sample loss $\widehat{\ell}(\cdot)$ by blockwise optimization, cycling through Riemannian gradient descent updates of $\boldsymbol{\theta}_1, \ldots, \boldsymbol{\theta}_N$ and Quasi-Newton updates of $\alpha_2, \ldots, \alpha_K$.

Riemannian gradient descent updates of $\boldsymbol{\theta}_1, \ldots, \boldsymbol{\theta}_N$ We update the positions $\boldsymbol{\theta}_1, \ldots, \boldsymbol{\theta}_N \in \mathcal{L}$ of units $1, \ldots, N$ by minimizing $\widehat{\ell}(\cdot)$ using Riemannian gradient descent (Absil et al., 2008, Chapter 4). At iteration $t + 1$, we update the position $\boldsymbol{\theta}_i^{(t)}$ of unit i to

$$\boldsymbol{\theta}_i^{(t+1)} \;=\; \exp_{\boldsymbol{\theta}_i^{(t)}}\left(-\eta_i^{(t+1)} \operatorname{proj}_{\boldsymbol{\theta}_i^{(t)}}(\boldsymbol{\vartheta}_i)\right),$$

where $\boldsymbol{\vartheta}_i \coloneqq \boldsymbol{J}\, \nabla_{\boldsymbol{\theta}_i} \widehat{\ell}(\boldsymbol{\Lambda})|_{\boldsymbol{\theta}_i = \boldsymbol{\theta}_i^{(t)}}$. The gradient $\nabla_{\boldsymbol{\theta}_i} \widehat{\ell}(\boldsymbol{\Lambda})$ is derived in Supplement B.1. The functions $\exp_{\boldsymbol{\theta}}(\boldsymbol{x})$ and $\operatorname{proj}_{\boldsymbol{\theta}}(\boldsymbol{x})$ refer to the exponential map and the orthogonal projection onto the tangent space of $\boldsymbol{\theta}$ with respect to the Lorentz model:

$$\begin{aligned}\exp_{\boldsymbol{\theta}}(\boldsymbol{x}) &\coloneqq \cosh(\langle \boldsymbol{x}, \boldsymbol{x} \rangle_{\mathcal{L}})\, \boldsymbol{\theta} + \frac{\sinh(\langle \boldsymbol{x}, \boldsymbol{x} \rangle_{\mathcal{L}})\, \boldsymbol{x}}{\langle \boldsymbol{x}, \boldsymbol{x} \rangle_{\mathcal{L}}} \\ \operatorname{proj}_{\boldsymbol{\theta}}(\boldsymbol{x}) &\coloneqq \boldsymbol{x} + \langle \boldsymbol{\theta}, \boldsymbol{x} \rangle_{\mathcal{L}}\, \boldsymbol{\theta}.\end{aligned}$$

The learning rate $\eta_i^{(t+1)} \in [0, \infty)$ is computed using the algorithm of Brent (1971). The algorithm ensures that $\widehat{\ell}(\cdot)$ is non-increasing.

Quasi-Newton updates of $\alpha_2, \ldots, \alpha_K$ We update sparsity parameters $\alpha_2, \ldots, \alpha_K$ by minimizing $\widehat{\ell}(\cdot)$. Setting the partial derivative of $\widehat{\ell}(\cdot)$ with respect to α_k to 0 gives

$$\sum_{e \in \mathcal{S}_k^{(0)} \cup \mathcal{S}_k^{(1)}} \frac{1}{\mu_e} \left(\frac{z_e}{\alpha_k} - \frac{\sigma\left(-g(\boldsymbol{\Theta}_e)\right)(1 - z_e)}{1 - \alpha_k\, \sigma\left(-g(\boldsymbol{\Theta}_e)\right)} \right) \;=\; 0,$$

which can be solved using the Quasi-Newton method of Byrd et al. (1995) subject to the constraint $\alpha_k \in (0,\, 1]$ $(k = 2, \ldots, K)$.

Convergence criterion We declare convergence when $|\widehat{\ell}(\mathbf{\Lambda}_t) - \widehat{\ell}(\mathbf{\Lambda}_{t+1})| \,/\, |\widehat{\ell}(\mathbf{\Lambda}_{t+1})| < 10^{-5}$, where $\mathbf{\Lambda}_t$ and $\mathbf{\Lambda}_{t+1}$ are the values of $\mathbf{\Lambda}$ at iterations t and $t+1$.

Computational complexity Approximating $\ell(\cdot)$ by $\widehat{\ell}(\cdot)$ comes at a computational cost of $O(\mathcal{S}_{\max})$ operations, where $\mathcal{S}_{\max} \coloneqq \max_{2 \le k \le K} |\mathcal{S}_k^{(0)} \cup \mathcal{S}_k^{(1)}|$. Updating positions requires $O(N\, \mathcal{S}_{\max})$ operations, while updating sparsity parameters requires $O(\mathcal{S}_{\max})$ operations.

4.3 Simulating Hypergraphs

To complement the scalable learning methods in Section 4.2, we develop scalable simulation methods for generating hypergraphs, facilitating simulation studies and model assessment.

Direct simulation of hypergraphs requires enumerating all $\binom{N}{k}$ possible hyperedges e of size $k \in \{2, \ldots, K\}$, which may be infeasible when N and K are large. We propose a scalable method for generating hyperedges of size $k \in \{2, \ldots, K\}$ in two steps:

Step 1: Generate U_k, the number of hyperedges of size k.

Step 2: Conditional on $U_k = u_k$, generate u_k hyperedges of size k.

We describe these steps in turn.

Step 1: Generate the number of hyperedges U_k The number of hyperedges U_k of size k is distributed as

$$U_k \;\sim\; \text{Poisson-Binomial}(\pi(\alpha_k, \mathbf{\Theta}_e),\; e \in \mathcal{E}_k).$$

To generate U_k from Poisson-Binomial$(\pi(\alpha_k, \mathbf{\Theta}_e),\; e \in \mathcal{E}_k)$, one needs to evaluate the probabilities $\pi(\alpha_k, \mathbf{\Theta}_e)$ of all $\binom{N}{k}$ hyperedges e of size k, which may be infeasible when N

and k are large. A scalable alternative is suggested by Le Cam's theorem along with $\pi(\alpha_k, \boldsymbol{\Theta}_e) \leq \alpha_k$, which shows that the total variation distance between the Poisson-Binomial distribution $\mathbb{P}$ and the Poisson distribution $\mathbb{Q}$ with mean $\lambda_k \coloneqq \sum_{e \in \mathcal{E}_k} \pi(\alpha_k, \boldsymbol{\Theta}_e)$ vanishes as long as the hypergraph is sparse enough:

$$\|\mathbb{P} - \mathbb{Q}\|_{\mathrm{TV}} \;\leq\; \sum_{e \in \mathcal{E}_k} \pi(\alpha_k, \boldsymbol{\Theta}_e)^2 \;\leq\; \alpha_k^2 \, N^k \;=\; o(1),$$

provided that $\alpha_k = o(1/\sqrt{N^k})$. In other words, U_k can be generated from Poisson(λ_k) as long as the hypergraph is sparse enough. Denoting by $\rho_k(\alpha_k, \boldsymbol{\Theta})$ the average probability of hyperedges of size k, we can express the mean λ_k of Poisson(λ_k) as $\lambda_k = \rho_k(\alpha_k, \boldsymbol{\Theta}) \binom{N}{k}$. To estimate $\rho_k(\alpha_k, \boldsymbol{\Theta})$, we sample $S \ll N$ units and estimate the mean $\rho_k(\alpha_k, \boldsymbol{\Theta})$ by the corresponding sample mean $\widehat{\rho}_k(\alpha_k, \boldsymbol{\Theta})$. We then generate the number of hyperedges U_k from Poisson$(\widehat{\lambda}_k)$ with mean $\widehat{\lambda}_k \coloneqq \widehat{\rho}_k(\alpha_k, \boldsymbol{\Theta}) \binom{N}{k}$.

Step 2: Generate u_k hyperedges conditional on $U_k = u_k$ Conditional on $U_k = u_k$, we generate a candidate $e \in \mathcal{E}_k$ from proposal distribution $q(e) \coloneqq 1/\binom{N}{k}$ and accept it with probability $\pi(\alpha_k, \boldsymbol{\Theta}_e)/(C\, q(e)) = \pi(1, \boldsymbol{\Theta}_e)$, where $C \coloneqq \alpha_k \binom{N}{k}$ is a convenient upper bound on $\max_{e \in \mathcal{E}_k} \pi(\alpha_k, \boldsymbol{\Theta}_e)/q(e)$. We continue sampling until u_k hyperedges are accepted.

5 Theoretical Guarantees

We state theoretical guarantees for minimizers of the sample loss $\widehat{\ell}(\cdot)$ based on a sample of hyperedges $\mathcal{S} \coloneqq \bigcup_{k=2}^{K} \mathcal{S}_k$, consisting of samples $\mathcal{S}_k \coloneqq \mathcal{S}_k^{(0)} \cup \mathcal{S}_k^{(1)}$ of hyperedges of size k $(k = 2, \ldots, K)$. We denote the minimizers of the sample loss $\widehat{\ell}(\cdot)$ by $\widehat{\boldsymbol{\Theta}}$ and $\widehat{\alpha}_2, \ldots, \widehat{\alpha}_K$, which are estimators of the true values $\boldsymbol{\Theta}^\star$ and $\alpha_2^\star, \ldots, \alpha_K^\star$. An estimator of the true Gram matrix $\boldsymbol{D}^\star \coloneqq \boldsymbol{\Theta}^\star \boldsymbol{J} (\boldsymbol{\Theta}^\star)^\top$ is $\widehat{\boldsymbol{D}} \coloneqq \widehat{\boldsymbol{\Theta}} \boldsymbol{J} \widehat{\boldsymbol{\Theta}}^\top$. We obtain theoretical guarantees under the following conditions.

Condition 1. *There exists a sequence of real numbers* $\rho_N \in (0,\, 1]$ *such that* $\alpha_k^\star \in [\rho_N,\, 1]$, *where* ρ_N *is a non-increasing function of* N.

Condition 2. *There exists a constant* $C_1 \in (0,\, \infty)$ *such that the elements* $\theta_{i,k}^\star$ *of* $\boldsymbol{\Theta}^\star$ *satisfy* $\max_{1\leq i\leq N} \max_{2\leq k\leq r+1} |\theta_{i,k}^\star| \leq C_1$.

Condition 3. *There exists a constant* $C_2 \in (1,\, \infty)$ *such that the elements* $D_{i,j}^\star$ *of* $\boldsymbol{D}^\star$ *satisfy* $\min_{1\leq i\neq j\leq N} D_{i,j}^\star \geq C_2$.

Condition 4. *There exist constants* $L_k \in (0,\, 1)$ *such that the sample inclusion probabilities* μ_e *satisfy* $\mu_e \geq L_k\, |\mathcal{S}_k| \,/\, |\mathcal{E}_k|$ *for all* $e \in \mathcal{E}_k$ $(k = 2, \ldots, K)$.

Condition 1 ensures that there are enough hyperedges to obtain theoretical guarantees, while allowing the hypergraph to be sparse. The sparsity of the hypergraph is controlled by ρ_N: If ρ_N is constant, the hypergraph is dense, whereas $\rho_N = o(1)$ implies that the hypergraph is sparse, in the sense that the expected number of hyperedges of size k can be of a smaller order of magnitude than the number of possible hyperedges $\binom{N}{k}$ $(k = 2, \ldots, K)$. Condition 2 is standard and requires that the units reside in a compact set. Condition 3 implies that units are well-separated. Condition 4 guarantees that all hyperedges have a positive probability of being included in the sample. The following theoretical guarantees assume that the size of the largest hyperedge K and the dimension r of hyperbolic space are constants, independent of the number of units N and the sample size of hyperedges $|\mathcal{S}|$.

The main result is Theorem 1, which considers the non-asymptotic scenario in which the number of units N is fixed and finite, whereas the sample size $|\mathcal{S}_k|$ of hyperedges of size k can grow until it reaches its finite upper bound $\binom{N}{k}$ $(k = 2, \ldots, K)$.

Theorem 1 *Consider any* $\epsilon \in (0, 1)$ *and any* $N \in \{3, 4, \ldots\}$. *Then, under Conditions 1–4, the following non-asymptotic error bounds hold with probability at least* $1 - \epsilon$*:*

$$\frac{1}{N(N-1)} \left\| \widehat{\boldsymbol{D}} - \boldsymbol{D}^\star \right\|_F^2 \;\leq\; C_3 \left[\sum_{k=2}^{K} \frac{L_k\, |\mathcal{S}_k|}{|\mathcal{S}|} \right]^{-1} \frac{\Delta_{N,r}}{\epsilon\, \rho_N^2\, \sqrt{|\mathcal{S}|}}$$

and

$$|\widehat{\alpha}_k - \alpha_k^\star| \;\leq\; C_4 \frac{\sqrt{|\mathcal{S}|}\,\Delta_{N,r}}{\epsilon\,\rho_N\,L_k\,|\mathcal{S}_k|}, \quad k = 2, \ldots, K,$$

where

$$\Delta_{N,r} \;\coloneqq\; \sqrt{(N\,r + K - 1)\,(K + 4)\,(K + 1)}$$

and $C_3 > 0$ *and* $C_4 > 0$ *are constants.*

A proof of Theorem 1 can be found in Supplement A.2. The first part of Theorem 1 establishes the rate of convergence of $\widehat{\boldsymbol{D}}$ as a function of the sample size $|\mathcal{S}_k|$ of hyperedges of size k ($k = 2, \ldots, K$), the total sample size $|\mathcal{S}| = \sum_{k=2}^{K} |\mathcal{S}_k|$, and the level of sparsity ρ_N. While there are no existing theoretical guarantees for hyperbolic space models of hypergraphs, it is instructive to compare Theorem 1 to theoretical results based on graphs. Assuming that ρ_N is constant so that the hypergraph is dense, the rate of convergence is $O(\sqrt{N/\,|\mathcal{S}|})$; note that the term $\sum_{k=2}^{K} (L_k\,|\mathcal{S}_k|)/|\mathcal{S}|$ is contained in the interval $[\min_{2\leq k\leq K} L_k,\, \max_{2\leq k\leq K} L_k]$ and $\Delta_{N,r} \asymp \sqrt{N}$ because K, $L_2, \ldots, L_K$, and r are constants. In the special case of graphs, the rate $O(\sqrt{N\,/\,|\mathcal{S}|})$ is known to be near-optimal (Davenport et al., 2014; Li et al., 2023). The second part of Theorem 1 establishes non-asymptotic error bounds on $\widehat{\alpha}_k$ in terms of $|\mathcal{S}_k|$ ($k = 2, \ldots, K$), $|\mathcal{S}|$, and ρ_N.

Theorem 1 paves the way for establishing rates of convergence for estimators $\widehat{\boldsymbol{\Theta}}$ of the positions $\boldsymbol{\Theta}^\star$. As discussed in Section 3.2, the positions can be estimated up to rotations, so we assume that the true positions $\boldsymbol{\Theta}^\star$ satisfy $\boldsymbol{\Theta}^\star \coloneqq \boldsymbol{U}\,|\boldsymbol{S}|^{1/2}\boldsymbol{J}$. To state the rate of convergence of $\widehat{\boldsymbol{\Theta}}$, we first state an additional condition.

Condition 5. *The smallest positive eigenvalue of* $\boldsymbol{D}^\star$ *satisfies* $\lambda_2(\boldsymbol{D}^\star) \asymp N$.

Condition 5 implies that the positions do not degenerate to a geodesic in the hyperbolic space. Under Conditions 1–5, we can establish consistency of the estimator $\widehat{\boldsymbol{\Theta}}$ for the true positions $\boldsymbol{\Theta}^\star$ in two-dimensional hyperbolic space up to rotations. The consistency result

can be extended from two-dimensional to higher-dimensional hyperbolic spaces using tools for indefinite matrix eigenspace (Rubin-Delanchy et al., 2022).

Theorem 2 *Under Conditions 1–5, assuming that N and $|\mathcal{S}|$ increase without bound,*

$$\frac{1}{N} \inf_{\boldsymbol{R} \in \mathcal{R}} \| \widehat{\boldsymbol{\Theta}} \boldsymbol{R} - \boldsymbol{\Theta}^{\star} \|_F^2 \;\; = \;\; O_p \left(\frac{\Delta_{N,2}}{\rho_N^2 \sqrt{|\mathcal{S}|}} \right),$$

where $\mathcal{R} \coloneqq \{ \boldsymbol{R} \in \mathbb{R}^{3 \times 3} : \; \boldsymbol{R} \boldsymbol{J} \boldsymbol{R}^{\top} = \boldsymbol{J} \}$ is the set of hyperbolic rotation matrices.

A proof of Theorem 2 can be found in Supplement A.3. In contrast to Theorem 1, Theorem 2 considers the asymptotic regime in which N and $|\mathcal{S}|$ grow without bound. To ensure that $(1/N) \inf_{\boldsymbol{R} \in \mathcal{R}} \| \widehat{\boldsymbol{\Theta}} \boldsymbol{R} - \boldsymbol{\Theta}^{\star} \|_F^2$ is small with high probability for all large enough N, the sample size $|\mathcal{S}|$ must be at least $|\mathcal{S}| \gg N / \rho_N^4$ in light of $\Delta_{N,2} \asymp \sqrt{N}$, but it can be lower than the maximum sample size of $\binom{N}{2} + \ldots + \binom{N}{K} \asymp N^K$.

6 Simulation Study

We demonstrate that the theoretical results in Section 5 are supported by simulation results. We consider hyperedges of sizes 2, 3, and 4 (i.e., $K = 4$) and set $\alpha_2 = 5 \times 10^{-1}$, $\alpha_3 = 5 \times 10^{-4}$, and $\alpha_4 = 5 \times 10^{-6}$. The positions of N units on the two-dimensional Poincaré disk are generated as described in Supplement C. In each scenario, we generate 100 population hypergraphs using the method described in Section 4.3. For each generated population hypergraph, we sample hyperedges using the sampling design described in Section 4.1.

Number of unrealized hyperedges n We consider $N = 400$ units and assess the statistical error as a function of $n \in \{1, 5, 10, 15, 20\}$, i.e., the number of unrealized hyperedges sampled for each realized hyperedge. Figure 3 suggests that $n = 5$ strikes the best balance between statistical error and computing time when $N = 400$.

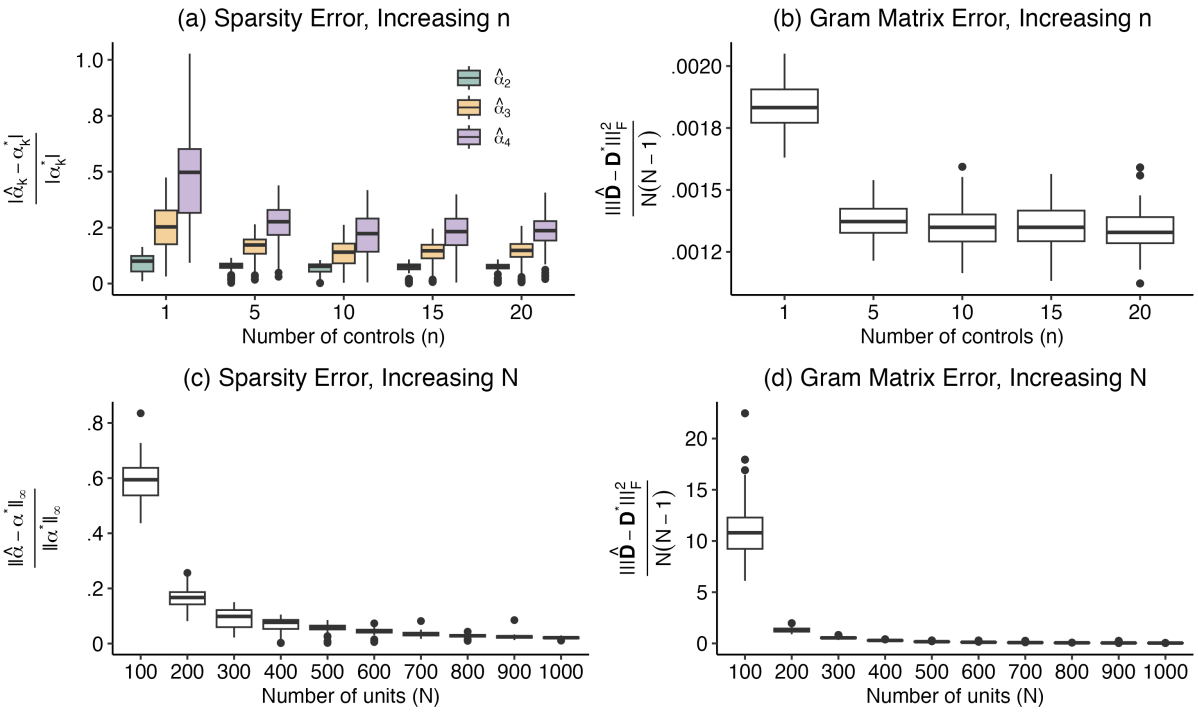

Figure 3: Simulation results: error of estimating sparsity parameter vector $\boldsymbol{\alpha} := (\alpha_2, \ldots, \alpha_K)^\top$ and Gram matrix $\boldsymbol{D}$ as a function of the number of controls n (the number of unrealized hyperedges sampled for each realized hyperedge) and the number of units N.

Number of units in hypergraph N To assess how the statistical error behaves as N increases, we consider $N \in \{100, 200, \ldots, 1{,}000\}$ and $n = 10$. The simulation results in Figure 3 support the theoretical results in Theorem 1: As N increases, the statistical error of estimating the Gram matrix $\boldsymbol{D}$ and the sparsity parameters $\alpha_2, \ldots, \alpha_K$ decreases.

7 Application to U.S. Newswire Articles

We showcase hyperbolic space models by applying them to U.S. Newswire articles between 1900 and 1977 (Silcock et al., 2014). Newswire articles by the Associated Press, Reuters, and other news organizations provide news sources for many local newspapers and form a comprehensive archive of publicly available information. We focus on the $N = 678$ U.S.

politicians who were mentioned at least five times in the U.S. Newswire data, who were born after 1900, and whose political affiliation is available. The number of realized hyperedges of size $k \in \{2, \ldots, N\}$ is: $|\mathcal{E}_2^{(1)}| = 4{,}624$, $|\mathcal{E}_3^{(1)}| = 2{,}815$, $|\mathcal{E}_4^{(1)}| = 1{,}208$, $|\mathcal{E}_5^{(1)}| = 607$, $|\mathcal{E}_6^{(1)}| = 261$, $|\mathcal{E}_7^{(1)}| = 104$, $|\mathcal{E}_8^{(1)}| = 70$, $|\mathcal{E}_9^{(1)}| = 20$, $|\mathcal{E}_{10}^{(1)}| = 3$, and $|\mathcal{E}_k^{(1)}| = 0$ for all $k \in \{11, \ldots, N\}$. Since hyperedges of sizes 2, 3, and 4 comprise 89% of the 9,712 realized hyperedges, we focus on hyperedges of sizes 2, 3, and 4 (i.e., $K = 4$). A more detailed description of the data is provided in Supplement D.1. While the entire hypergraph is observed, there are more than 8 billion possible hyperedges of sizes 2, 3, and 4. We thus sample hyperedges as described in Section 4.1, by sampling all realized hyperedges and sampling $n = 40$ unrealized hyperedges for each realized hyperedge.

We consider two-dimensional hyperbolic space to facilitate interpretation, and estimate the positions of politicians in hyperbolic space by conducting 100 estimation runs with starting values chosen at random, as described in Supplement B.3. All following results are based on the run minimizing $\widehat{\ell}(\cdot)$. We do not report comparisons with existing approaches for computational reasons: e.g., we were unable to obtain results using the approaches of Brusa and Matias (2024a,b), Turnbull et al. (2023), and Grose (2024) within 24 hours.

7.1 Estimated Positions

Figure 4 (a) shows the estimated positions $\boldsymbol{\Theta}$ of politicians on the Poincaré disk. Figure 4 (b) reveals that the politicians close to the center of the Poincaré disk were all political heavyweights between 1960 and 1977, the time frame for which we have most data. Many presidents and their vice presidents are close to each other, including Richard Nixon and Gerald Ford, John F. Kennedy and Lyndon B. Johnson, and Lyndon B. Johnson and Hubert Humphrey; note that Lyndon B. Johnson first served as vice president under President John F. Kennedy and then went on to serve as president after the assassination of President John F. Kennedy. So are the two Kennedy brothers (John F. and Robert F. Kennedy).

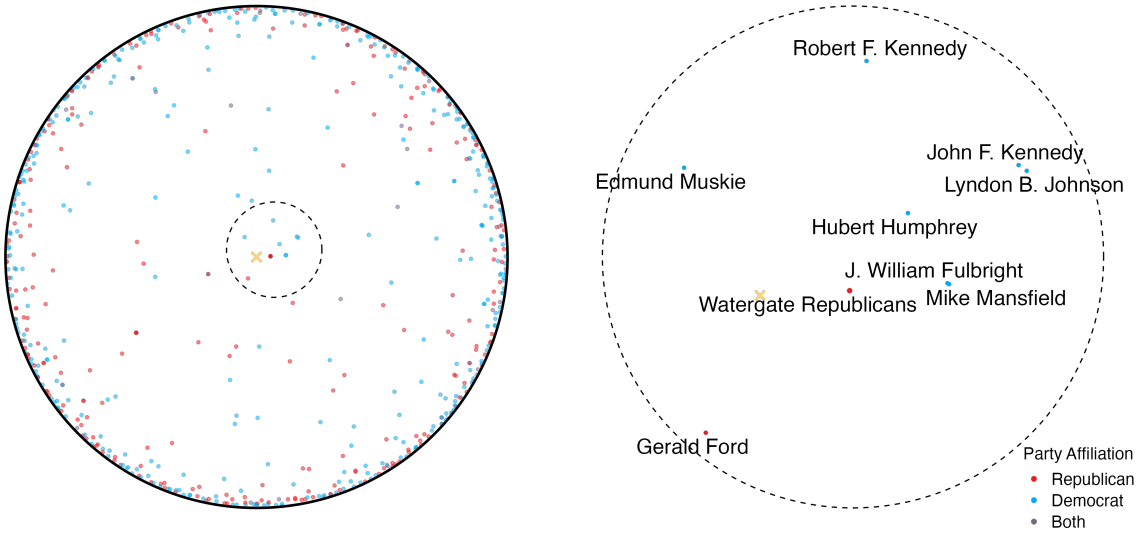

(a) Estimated positions of $N = 678$ politicians on the Poincaré disk.

(b) Estimated positions of the 13 politicians closest to the center of the Poincaré disk.

Figure 4: Newswire data: Estimated positions of politicians on the Poincaré disk, with party affiliation indicated by color; politicians who switched parties are labeled "both." The origin of the Poincaré disk is represented by ×. "Watergate Republicans" refers to Watergate era Republicans Richard Nixon, Henry Kissinger, Melvin Laird, Barry Goldwater, and Nelson Rockefeller, whose positions are almost indistinguishable.

7.2 Comparison of Hyperbolic and Euclidean Geometry

While the specification of $g(\cdot)$ in Equation (1) is based on hyperbolic distance, it can be extended to Euclidean distance as follows:

$$g_{\mathcal{E}}(\boldsymbol{\Theta}_e) \;\coloneqq\; \left\{ \frac{1}{|e|} \sum_{i \in e} \left[d^{(e)}_{\mathcal{E},i}(\boldsymbol{\Theta}_e) \right]^p \right\}^{1/p},$$

where

$$d^{(e)}_{\mathcal{E},i}(\boldsymbol{\Theta}_e) \;\coloneqq\; \sum_{j \in e \setminus \{i\}} \|\boldsymbol{\theta}_i - \boldsymbol{\theta}_j\|_2$$

is the Euclidean distance between $\boldsymbol{\theta}_i$ and $\boldsymbol{\theta}_j$. We compare results based on hyperbolic and Euclidean space models in terms of expressive power (hierarchical structure and embeddedness) and predictive power.

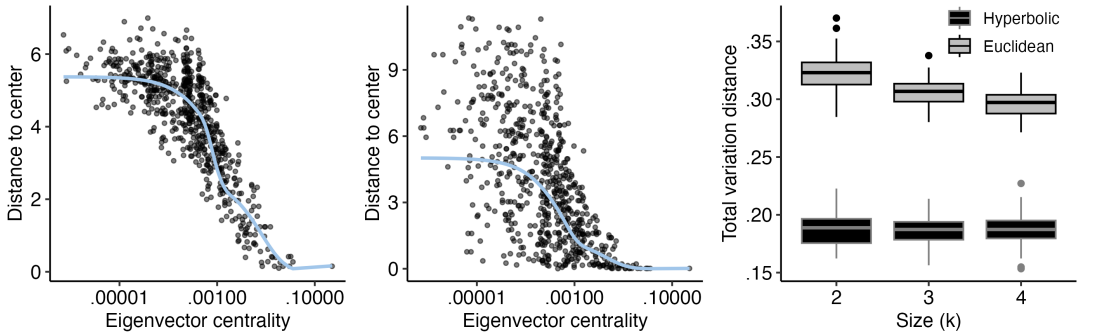

(a) Hyperbolic (R^2: .805) (b) Euclidean (R^2: .527) (c) TV size-k degree distribution

Figure 5: Newswire data: distances of politicians to the center of (a) hyperbolic space or (b) Euclidean space plotted against eigenvector centrality scores. The blue lines in (a) and (b) represent the smoothed averages of the distance to the center by eigenvector centrality score. The R^2 value is calculated from the accuracy of using the blue line for predicting the distance to the center based on the eigenvector centrality. (c) Total variation distance between the size-k degree distributions of observed and 100 simulated hypergraphs.

Expressive power We assess the expressive power of hyperbolic and Euclidean space models by comparing how these geometric models capture the hierarchical structure and the embeddedness of politicians.

A measure of unit-specific hierarchy in hypergraphs is the eigenvector centrality score of Bonacich et al. (2004). The eigenvector centrality scores are the coordinates of the normalized leading eigenvector of $\boldsymbol{A}^\top \boldsymbol{A}$, where $\boldsymbol{A} = (A_{m,i}) \in \{0,1\}^{M \times N}$ is the incidence matrix of the hypergraph, M is the number of realized hyperedges, and $A_{m,i} \coloneqq 1$ indicates that hyperedge m includes unit i and $A_{m,i} \coloneqq 0$ otherwise. To compute the distances of politicians to the center of the space, we compute the hyperbolic distance to the origin $(0,0) \in \mathbb{R}^2$ of the Poincaré disk and the Euclidean distance to the centroid of the positions of politicians. Figure 5 reveals how well each model can represent the hierarchy as quantified by eigenvector centrality scores. Under hyperbolic space models, politicians with high eigenvector centrality scores are close to the center of the Poincaré disk, whereas under

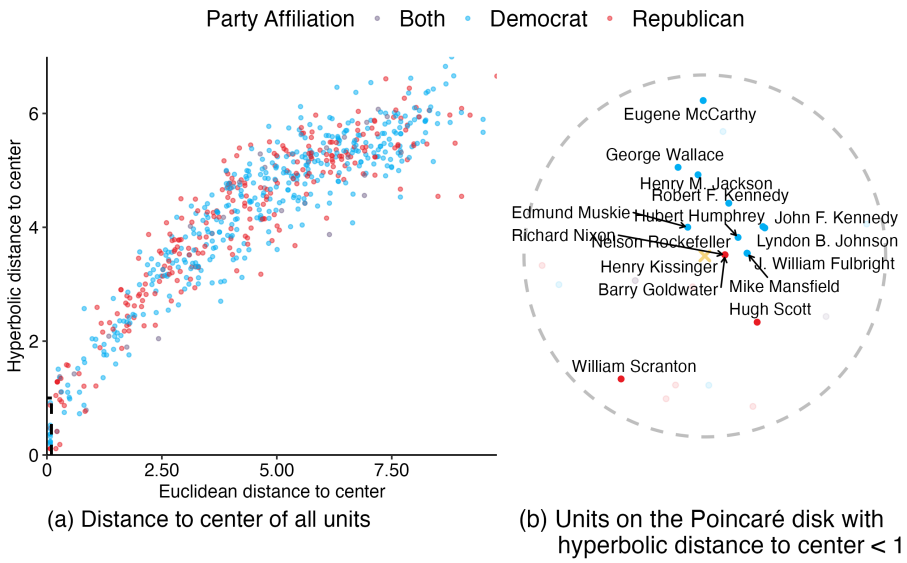

(a) Distance to center of all units

(b) Units on the Poincaré disk with hyperbolic distance to center < 1

Figure 6: (a) Hyperbolic and Euclidean distances of politicians to the center of the respective space. The dotted rectangle in (a) contains politicians with Euclidean distance of less than 1/10 to the center. (b) Positions of units with estimated hyperbolic distance less than 1 on the Poincaré disk. The politicians contained in the dotted rectangle in (a) are singled out and named in (b). The party affiliation of politicians is indicated by color; politicians who switched parties are labeled "both."

Euclidean space models some politicians with high eigenvector centrality scores are far from the center of the Euclidean space. Figure 6 (a) reveals that there is a positive but nonlinear relationship between the hyperbolic and Euclidean distances of units to the center of the respective space. The dashed rectangle in Figure 6 (a) highlights a small subset of politicians whose distances to the center according to the Euclidean geometry are less than 1/10. Figure 6 (b) displays the positions of those politicians on the Poincaré disk and provides the names of the politicians involved. These politicians, all political heavyweights of the twentieth century, are approximately equally close to the center of Euclidean space, but hyperbolic space differentiates among them in terms of political hierarchy (distance to the center) and political orientation (angle). For example, the Poincaré disk reveals that

politicians are separated by party lines: Democrats tend to be located in the upper semi-circle, while most Republicans are located in the lower semi-circle. At the center of the Poincaré disk sits President Nixon, surrounded by Democratic figures such as Humphrey and Muskie — the presidential and vice presidential candidates defeated by President Nixon and his Vice President Agnew in the presidential elections of 1968.

To assess how well the models capture the embeddedness of politicians in the hypergraph, we compare the size-k degree distribution of the observed hypergraph to the size-k degree distributions of 100 hypergraphs simulated from hyperbolic and Euclidean space models. The size-k degree distribution is defined as the empirical distribution of unit-specific size-k-degrees, where the size-k degree of a politician is the number of hyperedges of size k in which the politician is involved. The total variation distance between the observed and simulated size-k degree distributions in Figure 5 (c) suggests that hyperbolic space models capture the embeddedness of politicians in the hypergraph considerably better than Euclidean space models.

Predictive power To assess the out-of-sample performance of the model, we divide the realized hyperedges of sizes 2, 3, and 4 at random into training and test hyperedges encompassing 80% and 20% of the data, respectively. We use Precision-Recall (PR) and Receiver Operating Characteristic (ROC) curves to compare the performance of hyperbolic and Euclidean space models in Figure 7. The PR curves in the first row plot precision, the proportion of predicted positive hyperedges that are true positives, against recall, the proportion of true positive hyperedges correctly identified. The ROC curves in the second row plot recall (sensitivity) against specificity, the proportion of negatives incorrectly classified as positives. Figure 7 suggests that hyperbolic space models have a slight edge over Euclidean space models in terms of predictive power.

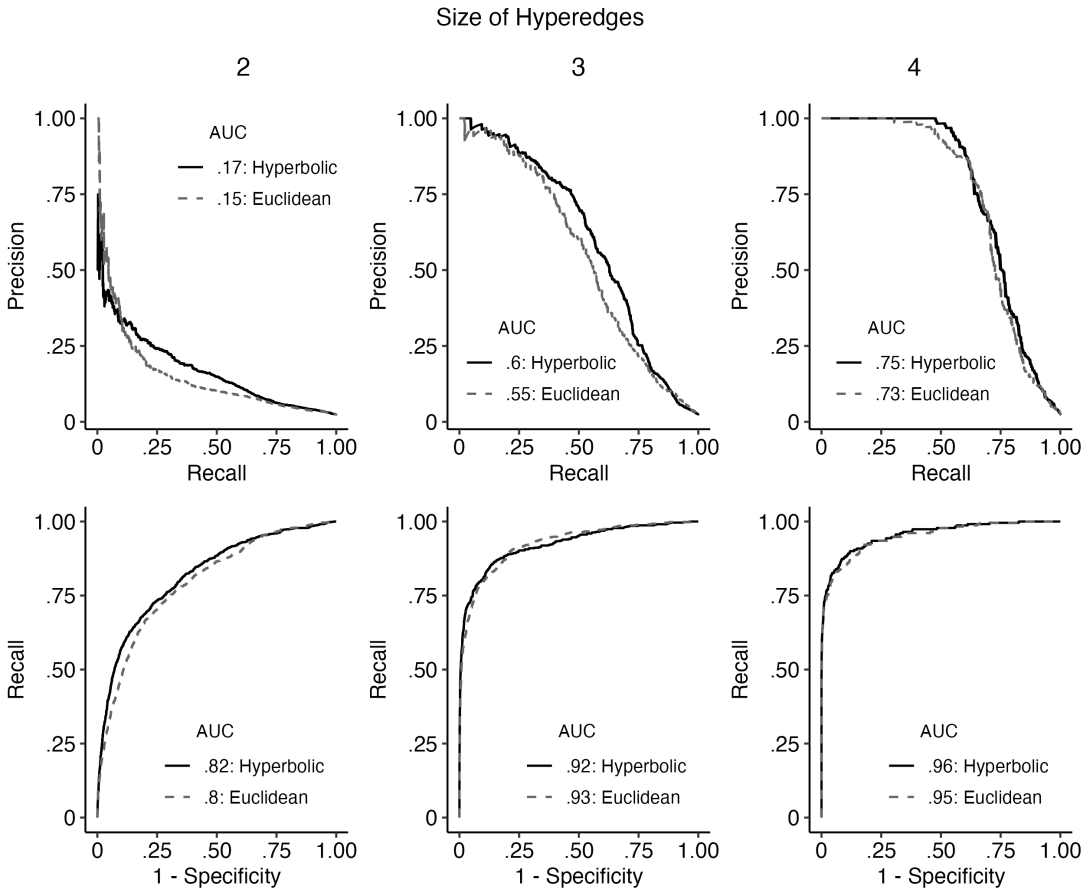

Figure 7: Newswire data: Receiver-Operator Characteristic (ROC) and Precision-Recall (PR) curve of out-of-sample predictions of hyperedges, based on embedding U.S. politicians in hyperbolic and Euclidean space.

8 Discussion

The Newswire data demonstrate that the choice of geometry matters: Hyperbolic space is superior to Euclidean space in its ability to represent core-periphery and local structure in the Newswire data. That said, the choice of geometry is less important for the purpose of predicting hyperedges in the Newswire data. An interesting direction for future research is incorporating attributes (e.g., party affiliation) to improve predictive power.

9 Data Availability Statement

The data used in Section 7 will be made publicly available.

Acknowledgements

The authors acknowledge support in the form of U.S. Department of Defense award ARO W911NF-21-1-0335 and U.S. National Science Foundation award NSF DMS-2515763.

References

Absil, P.-A., R. Mahony, and R. Sepulchre (2008). *Optimization Algorithms on Matrix Manifolds*. Princeton: Princeton University Press.

Bonacich, P., A. C. Holdren, and M. Johnston (2004). Hyper-edges and multidimensional centrality. *Social Networks 26*, 189–203.

Boumal, N. (2023). *An Introduction to Optimization on Smooth Manifolds*. Cambridge University Press.

Brent, R. P. (1971). An algorithm with guaranteed convergence for finding a zero of a function. *The Computer Journal 14*, 422–425.

Brusa, L. and C. Matias (2024a). Model-based clustering in simple hypergraphs through a stochastic blockmodel. *Scandinavian Journal of Statistics 51*, 1661–1684.

Brusa, L. and C. Matias (2024b). R package HyperSBM. Available at https://github.com/LB1304/HyperSBM.

Byrd, R. H., P. Lu, J. Nocedal, and C. Zhu (1995). A limited memory algorithm for bound constrained optimization. *SIAM Journal on Scientific Computing 16*, 1190–1208.

Clauset, A., C. Moore, and M. Newman (2008). Hierarchical structure and the prediction of missing links in networks. *Nature 453*, 98–10.

Davenport, M. A., Y. Plan, E. Van Den Berg, and M. Wootters (2014). 1-bit matrix completion. *Information and Inference 3*, 189–223.

Ghoshdastidar, D. and A. Dukkipati (2014). Consistency of spectral partitioning of uniform hypergraphs under planted partition model. *Advances in Neural Information Processing Systems 27*, 1–9.

Grose, D. (2024). R package Hyperlatent. Available at https://github.com/grosed/hyperlatent.

Kim, S., D. Lee, Y. Kim, J. Park, T. Hwang, and K. Shin (2023). Datasets, tasks, and training methods for large-scale hypergraph learning. *Data Mining and Knowledge Discovery 37*, 2216–2254.

Kim, S., S. Y. Lee, Y. Gao, A. Antelmi, M. Polato, and K. Shin (2024). A survey on hypergraph neural networks: An in-depth and step-by-step guide. In *ACM SIGKDD Conference on Knowledge Discovery and Data Mining*, pp. 6534–6544.

Kolaczyk, E. D. (2017). *Topics at the Frontier of Statistics and Network Analysis: (Re)Visiting the Foundations*. Cambridge University Press.

Krioukov, D., F. Papadopoulos, M. Kitsak, A. Vahdat, and M. Boguñá (2010). Hyperbolic geometry of complex networks. *Physical Review E 82*, 036106.

Li, J., G. Xu, and J. Zhu (2023). Hyperbolic network latent space model with learnable curvature. *Available at arXiv:2312.05319*.

Li, T., L. Lei, S. Bhattacharyya, K. van den Berge, P. Sarkar, P. J. Bickel, and E. Levina (2022). Hierarchical community detection by recursive partitioning. *Journal of the American Statistical Association 117*, 951–968.

Lubold, S., A. G. Chandrasekhar, and T. H. McCormick (2023). Identifying the latent space geometry of network models through analysis of curvature. *Journal of the Royal Statistical Society Series B: Statistical Methodology 85*, 240–292.

Lyu, Z., D. Xia, and Y. Zhang (2023). Latent space model for higher-order networks and generalized tensor decomposition. *Journal of Computational and Graphical Statistics 32*, 1320–1336.

Maleki, S., D. Saless, D. P. Wall, and K. Pingali (2022). HyperNetVec: Fast and Scalable Hierarchical Embedding for Hypergraphs. In P. Ribeiro, F. Silva, J. F. Mendes, and R. Laureano (Eds.), *Network Science*, Volume 13197, pp. 169–183.

Nandy, S. and B. B. Bhattacharya (2024). Degree heterogeneity in higher-order networks: Inference in the hypergraph β-model. *IEEE Transactions on Information Theory 70*, 6000–6024.

Ng, T. L. J. and T. B. Murphy (2022). Model-based clustering for random hypergraphs. *Advances in Data Analysis and Classification 16*, 1–33.

Nickel, M. and D. Kiela (2017). Poincaré embeddings for learning hierarchical representations. *Advances in Neural Information Processing Systems 30*, 1–10.

Nickel, M. and D. Kiela (2018). Learning continuous hierarchies in the Lorentz model of hyperbolic geometry. In *International Conference on Machine Learning*, pp. 3779–3788.

Rubin-Delanchy, P., J. Cape, M. Tang, and C. E. Priebe (2022). A statistical interpretation

of spectral embedding: the generalised random dot product graph. *Journal of the Royal Statistical Society Series B: Statistical Methodology 84*, 1446–1473.

Schweinberger, M., P. N. Krivitsky, C. T. Butts, and J. R. Stewart (2020). Exponential-family models of random graphs: Inference in finite, super, and infinite population scenarios. *Statistical Science 35*, 627–662.

Silcock, E., A. Arora, L. D'Amico-Wong, and M. Dell (2014). Newswire: A large-scale structured database of a century of historical news. In *Advances in Neural Information Processing Systems*, pp. 1–12.

Smith, A. L., D. M. Asta, and C. A. Calder (2019). The geometry of continuous latent space models for network data. *Statistical Science 34*, 428–453.

Tabaghi, P. and I. Dokmanić (2020). Hyperbolic distance matrices. In *ACM SIGKDD International Conference on Knowledge Discovery & Data Mining*, pp. 1728–1738.

Turnbull, K., S. Lunagómez, C. Nemeth, and E. Airoldi (2023). Latent space modeling of hypergraph data. *Journal of the American Statistical Association 119*, 1–13.

Yu, X. and J. Zhu (2025). Modeling hypergraphs with diversity and heterogeneous popularity. *Journal of the American Statistical Association*. To appear.

Yuan, M., R. Liu, Y. Feng, and Z. Shang (2022). Testing community structure for hypergraphs. *The Annals of Statistics 50*, 147–169.

Yuan, Y. and A. Qu (2023). High-order joint embedding for multi-level link prediction. *Journal of the American Statistical Association 118*, 1692–1706.

Supplementary Materials

A Proofs 2

A.1 Proof of Proposition 1 2

A.2 Proof of Theorem 1 3

A.3 Proof of Theorem 2 13

B Computational Details 17

B.1 Manifold Gradient Descent 17

B.2 Estimation under Euclidean Geometry 20

B.3 Initialization 21

C Simulating Positions 21

D Application to Newswire Data 22

D.1 Data 22

D.2 Additional Results of Euclidean and Hyperbolic Model 23

D.3 Sensitivity Analyses 27

E Computational Settings 31

A Proofs

A.1 Proof of Proposition 1

We first establish identifiability of the Gram matrix $\boldsymbol{D}$ and the sparsity parameters $\alpha_2, \ldots, \alpha_K$.

Proposition 1 *The Gram matrix $\boldsymbol{D} \coloneqq \boldsymbol{\Theta}\, \boldsymbol{J}\, \boldsymbol{\Theta}^\top$ and the sparsity parameters $\alpha_2, \ldots, \alpha_K$ are identifiable provided that $N > r + 2$.*

Consider any $k \in \{3, \ldots, K\}$. Let $f : \mathbb{R} \mapsto \mathbb{R}$ be defined by $f(y) \coloneqq \alpha \, \frac{2\exp(x)}{1+\exp(x)} - \frac{2\exp(y\,x)}{1+\exp(y\,x)}$, where $x \in \mathbb{R}$ is fixed. For any $\alpha \in (0,\, 1]$ and $x < 0$, we have $\frac{\partial f(y)}{\partial y} > 0$, $f(0) < 0$, and $f(+\infty) > 0$. Therefore, for a given α_k, we can find a corresponding $\widetilde{\alpha}_e$ such that

$$\pi(\alpha_{|e|}, \boldsymbol{\Theta}_e) \;\; = \;\; \alpha_k \, \sigma(-g(e)) \;\; = \;\; \sigma(-\widetilde{\alpha}_e \, g(e)),$$

where $\sigma(x) \coloneqq 2\, \exp(x)/(1 + \exp(x))$ and $g(e)$ is defined by

$$g(\boldsymbol{\Theta}_e) \;\coloneqq\; \left(\frac{1}{|e|} \sum_{i \in e} \left(\sum_{j \in e,\, j \neq i} d_{\mathcal{L}}(\boldsymbol{\theta}_i,\, \boldsymbol{\theta}_j) \right)^p \right)^{1/p}. \tag{A.1}$$

If there exists another set of sparsity parameters β_k and Gram matrix $\widetilde{\boldsymbol{D}}$ such that

$$\alpha_k \, \sigma(-g(e)) \;\; = \;\; \beta_k \, \sigma(-\widetilde{g}(e)),$$

then we obtain, for some $\widetilde{\beta}_e$,

$$\sigma(\widetilde{\alpha}_e \, g(e)) \;\; = \;\; \sigma(\widetilde{\beta}_e \, \widetilde{g}(e)),$$

where $\widetilde{g}(e)$ is defined by

$$\widetilde{g}(e) \;\; \coloneqq \;\; \left(\frac{1}{|e|} \sum_{i \in e} \operatorname{arcosh}(-\widetilde{D}_{i,j})^p \right)^{1/p}.$$

In other words, we have an overdetermined system with $O(N^k)$ equations involving $O(N^2)$ variables $\operatorname{arcosh}(-\widetilde{\boldsymbol{D}})$. The equations hold only when $\alpha_k = \beta_k$ and $\operatorname{arcosh}(-\boldsymbol{D}) = \operatorname{arcosh}(-\widetilde{\boldsymbol{D}})$. Since the $\operatorname{arcosh}(\cdot)$ is a monotone function, we obtain $\boldsymbol{D} = \widetilde{\boldsymbol{D}}$.

Last, but not least, consider the case $K = 2$. For another set of sparsity parameters β_2 and Gram matrix $\widetilde{\boldsymbol{D}} = \widetilde{\boldsymbol{\Theta}}\boldsymbol{J}\widetilde{\boldsymbol{\Theta}}^\top$, we obtain

$$\alpha_2\,\sigma\left(-\text{arcosh}(-\boldsymbol{\Theta}\boldsymbol{J}\boldsymbol{\Theta}^\top)\right) \;=\; \beta_2\,\sigma\left(-\text{arcosh}(-\widetilde{\boldsymbol{\Theta}}\boldsymbol{J}\widetilde{\boldsymbol{\Theta}}^\top)\right).$$

Since $\boldsymbol{\Theta}$, $\widetilde{\boldsymbol{\Theta}} \in \mathbb{R}^{N\times(r+1)}$ and the function $\text{arcosh}(\cdot)$ is monotonic, we obtain $N\,(N-1)$ equations involving $N\,(r+1)$ variables. If $N > r+2$, then $\alpha_2 = \beta_2$ and $\boldsymbol{D} = \widetilde{\boldsymbol{D}}$, completing the proof.

A.2 Proof of Theorem 1

Theorem 1 *Consider any $\epsilon \in (0,1)$ and any $N \in \{3,4,\ldots\}$. Then, under Conditions 1–4, the following non-asymptotic error bounds hold with probability at least $1-\epsilon$:*

$$\frac{1}{N(N-1)}\,\|\!|\widehat{\boldsymbol{D}} - \boldsymbol{D}^\star|\!\|_F^2 \;\leq\; C\left[\sum_{k=2}^{K}\frac{|\mathcal{S}_k|\,L_k}{|\mathcal{S}|}\right]^{-1}\frac{\Delta_{N,r}}{\epsilon\,\rho_N^2\,\sqrt{|\mathcal{S}|}}$$

and

$$|\widehat{\alpha}_k - \alpha_k^\star| \;\leq\; C'\,\frac{\sqrt{|\mathcal{S}|}\;\Delta_{N,r}}{\epsilon\,\rho_N\,L_k\,|\mathcal{S}_k|},\quad k = 2,\ldots,K,$$

where

$$\Delta_{N,r} \;\coloneqq\; \sqrt{(N\,r+K-1)\,(K+4)\,(K+1)}$$

and $C > 0$ and $C' > 0$ are constants independent of N.

In the following, we denote $C(k) = \binom{N}{k}$. Denote possible latent positions and sparsity parameters as $\boldsymbol{\Theta}$ and $\boldsymbol{\alpha}$, and the corresponding Gram matrix $\boldsymbol{D} \in \mathbb{R}^{N\times N}$. The true values are denoted by $\boldsymbol{\Theta}^\star$, $\boldsymbol{\alpha}^\star$, and $\boldsymbol{D}^\star = \boldsymbol{\Theta}^\star\boldsymbol{J}\,(\boldsymbol{\Theta}^\star)^\top$, while the minimizers of the sample loss $\widehat{\ell}(\cdot)$ are $\widehat{\boldsymbol{\Theta}}$, $\widehat{\boldsymbol{\alpha}}$, and $\widehat{\boldsymbol{D}}$. We define the multivariate function $f_k(\boldsymbol{D}) = \{f_k^{(e)}(\boldsymbol{D})\}_{e\in\mathcal{E}_k} : \mathbb{R}^{N\times N} \mapsto [0,\,1]^{C(k)}$, where, for all $e \in \mathcal{E}_k$,

$$f_k^{(e)}(\boldsymbol{D}) \;\coloneqq\; \sigma(-g(\boldsymbol{\Theta}_e)) \tag{A.2}$$

is the vector of probabilities corresponding to all possible hyperedges of size $k \in \{2, ..., K\}$ if the sparsity parameters $\alpha_2, ..., \alpha_K$ are set to 1. The function g is given in Equation (A.1), which can be perceived as a function of $\boldsymbol{D}$ in Equation (A.2). To emphasize the dependence of probability on nodes in e and for a better illustration, we introduce the following notation for the probability to observe $e = (i_1, i_2, \ldots, i_k) \in \mathcal{E}_k$ with $k = 2, \ldots, K$:

$$P_{i_1,\ldots,i_k} \;\coloneqq\; \alpha_k \, f_k^{(i_1,\ldots,i_k)}(\boldsymbol{D}). \tag{A.3}$$

Accordingly, hyperedge probability tensors are defined as follows

$$\boldsymbol{P}_k^\star \;\coloneqq\; \{P^\star_{i_1,\ldots,i_k}\}_{1\le i_1,\ldots,i_k\le N}, \qquad \widehat{\boldsymbol{P}}_k \;\coloneqq\; \{\widehat{P}_{i_1,\ldots,i_k}\}_{1\le i_1,\ldots,i_k\le N},$$

where $P^\star_{i_1,\ldots,i_k}$ and $\widehat{P}_{i_1,\ldots,i_k}$ result from plugging in $(\boldsymbol{D}^\star, \boldsymbol{\alpha}^\star)$ and $(\widehat{\boldsymbol{D}}, \widehat{\boldsymbol{\alpha}})$ into the probabilities defined in Equation (A.3).

Consider the joint loglikelihood function based on $\mathcal{S} = \cup_{k=2}^K \mathcal{S}_k$ collecting all sampled hyperedges of different sizes:

$$\sum_{e\in\mathcal{S}} \ell(Z_e \mid \widehat{\boldsymbol{D}}, \widehat{\boldsymbol{\alpha}}) = \sum_{k=2}^K \sum_{e\in\mathcal{S}_k} Z_e \log \widehat{\alpha}_k f_k(\widehat{\boldsymbol{D}}) + (1 - Z_e) \log(1 - \widehat{\alpha}_k f_k(\widehat{\boldsymbol{D}})).$$

We can write

$$\begin{aligned}
&\sum_{e\in\mathcal{S}} \Big[\ell(Z_e \mid \widehat{\boldsymbol{D}}, \widehat{\boldsymbol{\alpha}}) - \ell(Z_e \mid \boldsymbol{D}^\star, \boldsymbol{\alpha}^\star)\Big] \\
=\;& \sum_{k=2}^K \sum_{e\in\mathcal{S}_k} \Big[\ell_k(Z_e \mid \widehat{\boldsymbol{D}}, \widehat{\alpha}_k) - \mathbb{E}\,\ell_k(Z_e \mid \widehat{\boldsymbol{D}}, \widehat{\alpha}_k) \\
-\;& (\ell_k(Z_e \mid \boldsymbol{D}^\star, \alpha_k^\star) - \mathbb{E}\,\ell_k(Z_e \mid \boldsymbol{D}^\star, \alpha_k^\star)) \\
+\;& \mathbb{E}\,\ell_k(Z_e \mid \widehat{\boldsymbol{D}}, \widehat{\alpha}_k) - \mathbb{E}\,\ell_k(Z_e \mid \boldsymbol{D}^\star, \alpha_k^\star)\Big] \\
\le\;& \sum_{k=2}^K \sum_{e\in\mathcal{S}_k} \Big[\mathbb{E}\,\ell_k(Z_e \mid \widehat{\boldsymbol{D}}, \widehat{\alpha}_k) - \mathbb{E}\,\ell_k(Z_e \mid \boldsymbol{D}^\star, \alpha_k^\star)\Big] \\
+\;& \sup_{\boldsymbol{D},\boldsymbol{\alpha}} \left|\sum_{e\in\mathcal{S}_k} \ell(Z_e \mid \boldsymbol{D}, \boldsymbol{\alpha}) - \mathbb{E}\,\ell(Z_e \mid \boldsymbol{D}, \boldsymbol{\alpha})\right|
\end{aligned} \tag{A.4}$$

Note that the expectation is taken with respect to both $\{Z_e\}$ and the random sampling of hyperedges.

We use the Kullback–Leibler divergence to measure the discrepancy between hyperedge probability distribution, and introduce $\boldsymbol{Q}_k$ as the hyperedge probability tensor encompassing the probabilities defined in Equation (A.3) with $(\widehat{\boldsymbol{D}}, \boldsymbol{\alpha}^\star)$. The average KL-divergence and Hellinger distance for the m-size hypergraph are

$$\begin{aligned} D_k(\boldsymbol{P}_k^\star \| \widehat{\boldsymbol{P}}_k) &\coloneqq \frac{1}{C(k)} \sum_{1 \le i_1,\ldots,i_k \le N} P^\star_{i_1,\ldots,i_k} \log \frac{P^\star_{i_1,\ldots,i_k}}{\widehat{P}_{i_1,\ldots,i_k}} + (1 - P^\star_{i_1,\ldots,i_k}) \log \frac{(1 - P^\star_{i_1,\ldots,i_k})}{(1 - \widehat{P}_{i_1,\ldots,i_k})} \\ D_k^H(\boldsymbol{P}_k^\star \| \widehat{\boldsymbol{P}}_k) &\coloneqq \frac{1}{C(k)} \sum_{1 \le i_1,\ldots,i_k \le N} \left(\sqrt{P^\star_{i_1,\ldots,i_k}} - \sqrt{\widehat{P}_{i_1,\ldots,i_k}} \right)^2 \\ &+ \left(\sqrt{1 - P^\star_{i_1,\ldots,i_k}} - \sqrt{1 - \widehat{P}_{i_1,\ldots,i_k}} \right)^2, \end{aligned}$$

respectively. Note that $D_k(\boldsymbol{P}_k^\star \| \widehat{\boldsymbol{P}}_k) \ge D_k^H(\boldsymbol{P}_k^\star \| \widehat{\boldsymbol{P}}_k)$. Given that the sampling probability of a hyperedge $e = (i_1, \ldots, i_k)$ to be sampled in $\mathcal{S}_k$ is $\mu_e \ge L_k |\mathcal{S}_k| / C(k)$, we have

$$\begin{aligned} &-\mathbb{E}\left(\ell_k(\widehat{\boldsymbol{D}}, \widehat{\boldsymbol{\alpha}}) - \ell_k(\boldsymbol{D}^\star, \boldsymbol{\alpha}^\star)\right) = \mathbb{E}_{e \in \mathcal{S}_k} \mathbb{E}_{Z_e} \left\{ \ell_k(\boldsymbol{D}^\star, \boldsymbol{\alpha}^\star) - \ell_k(\widehat{\boldsymbol{D}}, \widehat{\boldsymbol{\alpha}}) \right\} \\ &= \sum_{1 \le i_1,\ldots,i_k \le N} \mu_e \Big\{ P^\star_{i_1,\ldots,i_k} \log \frac{P^\star_{i_1,\ldots,i_k}}{\widehat{P}_{i_1,\ldots,i_k}} + (1 - P^\star_{i_1,\ldots,i_k}) \log \frac{(1 - P^\star_{i_1,\ldots,i_k})}{(1 - \widehat{P}_{i_1,\ldots,i_k})} \Big\} \\ &\ge L_k |\mathcal{S}_k| D_k(\boldsymbol{P}_k^\star \| \widehat{\boldsymbol{P}}_k). \end{aligned}$$

Then we have

$$D_k(\boldsymbol{P}_k^\star \| \widehat{\boldsymbol{P}}_k) = D_k(\boldsymbol{P}_k^\star \| \boldsymbol{Q}_k) + \boldsymbol{D}_k^{(2)}(\boldsymbol{P}_k^\star, \widehat{\boldsymbol{P}}_k, \boldsymbol{Q}_k), \tag{A.5}$$

where

$$\begin{aligned} &\boldsymbol{D}_k^{(2)}(\boldsymbol{P}_k^\star, \widehat{\boldsymbol{P}}_k, \boldsymbol{Q}_k) = \\ &\frac{1}{C(m)} \sum_{1 \le i_1,\ldots,i_k \le N} P^\star_{i_1,\ldots,i_k} \log \frac{Q_{i_1,\ldots,i_k}}{\widehat{P}_{i_1,\ldots,i_k}} + (1 - P^\star_{i_1,\ldots,i_k}) \log \frac{(1 - Q_{i_1,\ldots,i_k})}{(1 - \widehat{P}_{i_1,\ldots,i_k})}. \end{aligned}$$

Based on Equation (2), there exist constants $0 < C_3 < C_4 < 1$ such that $f_k^{(i_1,\cdots,i_k)}(\boldsymbol{D}) \in [C_3, C_4]$ for $k \in \{2, \ldots, K\}$. Define $h(x) \coloneqq x_0 \log \frac{x_0}{x} + (1 - x_0) \log \frac{1 - x_0}{1 - x}$, where $0 < x < 1$ and $x_0 = \alpha_k^\star f_k^{(e)}(\boldsymbol{D}^\star)$, and denote $x_1 = \widehat{\alpha}_k f_k^{(e)}(\widehat{\boldsymbol{D}})$ and $x_2 = \alpha_k^\star f_k^{(e)}(\widehat{\boldsymbol{D}})$. Each term in

$D_k(\boldsymbol{P}_k^\star \| \widehat{\boldsymbol{P}}_k)$ and $D_k(\boldsymbol{P}_k^\star \| \boldsymbol{Q}_k^{(1)})$ can then be represented as $h(x_1)$ and $h(x_2)$. We compare $h(x_1)$ and $h(x_2)$ in the following. Note that

$$h'(x) \;=\; \frac{x - x_0}{x\,(1-x)} \text{ and } h''(x) \;=\; \frac{x^2 + x_0 - 2\,x_0\,x}{x^2\,(1-x)^2}.$$

We first perform Taylor expansion of $h(x_1)$ from x_0 and use the fact that $h(x_0) = 0, h'(x_0) = 0$, then $h(x_1) = \frac{x_1^2 + x_0 - 2x_0x_1}{x_1^2(1-x_1)^2}(x_1 - x_0)^2 + o_N(x_1 - x_0)^2 = \boldsymbol{\omega}_N(\widehat{\alpha}_k - \alpha_k^\star)^2$, where $a = \boldsymbol{\omega}_N(b)$ means that $|a(N)/b(N)| \geq C$ for large enough N for some constant $C > 0$. In the above claim, we use condition 1, where $\alpha_k \in [\rho_N, 1]$ can decreases as N increases. Similarly, $h(x_2) = h(x_1) + \frac{x_1 - x_0}{x_1(1-x_1)}(x_2 - x_1) + O_N(x_2 - x_1)^2 = h(x_1) + O_N(\frac{(\widehat{\alpha}_k - \alpha_k^\star)^2}{\widehat{\alpha}_k}) + O_N(\widehat{\alpha}_k - \alpha_k^\star)^2$. Then, by combining $h(x_1)$ and $h(x_2)$, we have

$$h(x_2)/h(x_1) \leq 1 + O_N\left(\frac{(\widehat{\alpha}_k - \alpha_k^\star)^2}{\widehat{\alpha}_k(\widehat{\alpha}_k - \alpha_k^\star)^2}\right) = O_N\left(\frac{1}{\widehat{\alpha}_k}\right) \leq \rho_N^{-1}.$$

Notice that $D_k(\boldsymbol{P}_k^\star \| \widehat{\boldsymbol{P}}_k) = \frac{1}{C(k)} \sum_{1 \leq i_1, \ldots, i_k \leq N} h(x_2)$ and $D_k(\boldsymbol{P}_k^\star \| \boldsymbol{Q}_k) = \frac{1}{C(k)} \sum_{1 \leq i_1, \ldots, i_k \leq N} h(x_1)$, Then we can apply the above arguments for different $k = 1, \ldots, K$ and have

$$D_k(\boldsymbol{P}_k^\star \| \boldsymbol{Q}_k) \;\leq\; \rho_N^{-1}\, D_k(\boldsymbol{P}_k^\star \| \widehat{\boldsymbol{P}}_k),\; k = 1, \cdots, K \tag{A.6}$$

Combining (A.5) and (A.6), we have

$$(1 - \rho_N^{-1}) D_k(\boldsymbol{P}_k^\star \| \widehat{\boldsymbol{P}}_k) \;\leq\; \boldsymbol{D}_k^{(2)}(\boldsymbol{P}_k^\star,\, \widehat{\boldsymbol{P}}_k,\, \boldsymbol{Q}_k) \;\leq\; D_k(\boldsymbol{P}_k^\star \| \widehat{\boldsymbol{P}}_k). \tag{A.7}$$

We define the multivariate function $F_k(\boldsymbol{D}) : \mathbb{R}^{N \times N} \mapsto [0,\, 1]^{C(k)}$ as

$$F_k(\boldsymbol{D}) \;\coloneqq\; \left\{ \sqrt{\tfrac{1}{C(k)} f_k^{(e)}(\boldsymbol{D})} \right\}_{e \in \mathcal{E}_k}.$$

Notice that $F_k(\boldsymbol{D})$ is an overdetermined system and $F_k(\boldsymbol{D}) = 0$ only when $\|\boldsymbol{D}\|_F \to \infty$ due that $\boldsymbol{D}_{i,j} > 0$ given Condition 3. Therefore, $F_k(\boldsymbol{D})$ is an injective and continuous mapping. Define a new norm on $\boldsymbol{D}$ as $\|\boldsymbol{D}\| := \|\boldsymbol{D}\|_F / \sqrt{C(2)}$ and then $\|\boldsymbol{D}\| = 1$ define a sphere $\|\boldsymbol{D}\|_F = \sqrt{C(2)}$. Given that compactness of $\|\boldsymbol{D}\| = 1$ and continuity of $F_k(\boldsymbol{D})$ over $\|\boldsymbol{D}\| = 1$, then there exists $c^{(1)} > 0$ such that $c^{(1)} = \inf_{\|\boldsymbol{D}\|=1} \|F_k(\boldsymbol{D})\|_F$. Given

Condition 3 that $\boldsymbol{D}_{i,j}$ is lower bounded, there exists constant C_3' such that $f_k^{(e)}(\boldsymbol{D}) \geq C_3'$ and $F_k(\boldsymbol{D})_{i_1,\cdots,i_k} \geq \sqrt{C_3'/C(k)}$ then $\|F_k(\boldsymbol{D})\|_F \geq \sqrt{C_3'}$ for all $\boldsymbol{D}$, then we have

$$\left\| F_k\left(\frac{\boldsymbol{D}}{\|\boldsymbol{D}\|}\right)\right\|_F \geq c^{(1)} \geq \sqrt{C_3'} \implies \|F_k(\boldsymbol{D})\|_F^2 \geq \frac{C_3'}{C(2)}\|\boldsymbol{D}\|_F^2.$$

Consider $\boldsymbol{D}^\star$ which also satisfies $\|F_k(\boldsymbol{D}^\star)\|_F^2 \geq \frac{C_3'}{C(2)}\|\boldsymbol{D}^\star\|_F^2$ and notice that

$$\frac{2}{C(k)}\sum_{e\in\mathcal{E}_k}\sqrt{f_k^e(\boldsymbol{D})f_k^e(\boldsymbol{D}^\star)} \leq 2 \leq \frac{2}{C(2)}\sum_{1\leq i,j\leq N}\boldsymbol{D}_{i,j}\boldsymbol{D}^\star_{i,j},$$

where we use the fact that $f_k^e(\boldsymbol{D}), f_k^e(\boldsymbol{D}^\star) \leq 1$ and $\boldsymbol{D}_{i,j}, \boldsymbol{D}^\star_{i,j} > 1$ by Condition 3. Then we have

$$\|F_k(\boldsymbol{D}) - F_k(\boldsymbol{D}^\star)\|_F^2 \;\; \geq \;\; \tfrac{C_3'}{C(2)}\|\boldsymbol{D} - \boldsymbol{D}^\star\|_F^2,$$

and, upon replacing $\boldsymbol{D}$ by $\widehat{\boldsymbol{D}}$, we obtain

$$\begin{aligned}
&\frac{1}{C(k)}\sum_{1\leq i_1,\ldots,i_k\leq N}\left(\sqrt{P^\star_{i_1,\ldots,i_k}} - \sqrt{Q_{i_1,\ldots,i_k}}\right)^2 \frac{1}{C(k)}\sum_{1\leq i_1,\ldots,i_k\leq N}\left(\sqrt{P^\star_{i_1,\ldots,i_k}} - \sqrt{Q_{i_1,\ldots,i_k}}\right)^2 \\
= \;\; & \alpha_k^\star\|F_k(\widehat{\boldsymbol{D}}) - F_k(\boldsymbol{D}^\star)\|_F^2 \;\geq\; \frac{C_3'\alpha_k^\star}{C(2)}\|\widehat{\boldsymbol{D}} - \boldsymbol{D}^\star\|_F^2 \geq \frac{C_3'\rho_N}{C(2)}\|\widehat{\boldsymbol{D}} - \boldsymbol{D}^\star\|_F^2.
\end{aligned} \tag{A.8}$$

Based on Taylor expansion on $h(x) = \sqrt{1-x_0} - \sqrt{1-x}$, we have for every $e = \{i_1, \cdots, i_k\}$

$$\left(\sqrt{1-P^\star_{i_1,\ldots,i_k}} - \sqrt{1-Q^{(1)}_{i_1,\ldots,i_k}}\right)^2 = \boldsymbol{\omega}_N((\alpha_k^\star)^2(f_k^{(e)}(\boldsymbol{D}^\star) - f_k^{(e)}(\widehat{\boldsymbol{D}}))^2)$$

Then by defining a multivariate function $\widetilde{F}_k(\boldsymbol{D}) : \mathbb{R}^{N\times N} \mapsto [0,1]^{C(k)}$ as

$$\widetilde{F}_k(\boldsymbol{D}) \;\coloneqq\; \left\{\sqrt{\tfrac{1}{C(k)}}f_k^{(e)}(\boldsymbol{D})\right\}_{e\in\mathcal{E}_k},$$

and following above argument above, we can again bound $\widetilde{F}_k(\boldsymbol{D})$ from below with some constant $C_3'' > 0$

$$\frac{1}{C(k)}\sum_{1\leq i_1,\ldots,i_k\leq N}\left(\sqrt{1-P^\star_{i_1,\ldots,i_k}} - \sqrt{1-\widehat{P}_{i_1,\ldots,i_k}}\right)^2 \geq \frac{C_3''\rho_N^2}{C(2)}\|\widehat{\boldsymbol{D}} - \boldsymbol{D}^\star\|_F^2. \tag{A.9}$$

Combining Equation (A.8) and Equation (A.9), we obtain, for some constant $C_4 > 0$,

$$D_k^H(\boldsymbol{P}_k^\star \| \boldsymbol{Q}_k) \;\; \geq \;\; \frac{C_4\, \rho_N}{C(2)} \| \widehat{\boldsymbol{D}} - \boldsymbol{D}^\star \|_F^2.$$

Noting that $D_k^H(\boldsymbol{P}_k^\star \| \boldsymbol{Q}_k) \leq D_k(\boldsymbol{P}_k^\star \| \boldsymbol{Q}_k) \leq \rho_N^{-1} D_k(\boldsymbol{P}_k^\star \| \widehat{\boldsymbol{P}}_k)$, we have for $k = 2, \ldots, K$,

$$D_k(\boldsymbol{P}_k^\star \| \widehat{\boldsymbol{P}}_k) \;\; \geq \;\; \frac{C_4\, \rho_N^2}{N(N-1)} \| \widehat{\boldsymbol{D}} - \boldsymbol{D}^\star \|_F^2. \tag{A.10}$$

Given $\sum_{e \in \mathcal{S}_k} \mathbb{E}\, \ell_k(Z_e \mid \widehat{\boldsymbol{D}}, \widehat{\boldsymbol{\alpha}}) - \mathbb{E}\, \ell_k(Z_e \mid \boldsymbol{D}^\star, \boldsymbol{\alpha}^\star) \leq -L_k |\mathcal{S}_k| D_k(\boldsymbol{P}_k^\star \| \widehat{\boldsymbol{P}}_k)$ and (A.10), we have

$$\begin{aligned}
& - \;\; \frac{1}{|\mathcal{S}|} \mathbb{E} \sum_{e \in \mathcal{S}} \big(\ell(Z_e \mid \widehat{\boldsymbol{D}}, \widehat{\boldsymbol{\alpha}}) - \ell(Z_e \mid \boldsymbol{D}^\star, \boldsymbol{\alpha}^\star) \big) \\
& = \;\; - \sum_{k=2}^{K} \frac{1}{|\mathcal{S}|} \mathbb{E} \big(\sum_{e \in \mathcal{S}_k} \ell_k(Z_e \mid \widehat{\boldsymbol{D}}, \widehat{\alpha}_k) - \ell_k(Z_e \mid \boldsymbol{D}^\star, \alpha_k^\star) \big) \\
& \geq \;\; \sum_{k=2}^{K} \frac{L_k |\mathcal{S}_k|}{|\mathcal{S}|} D_k(\boldsymbol{P}_k^\star \| \widehat{\boldsymbol{P}}_k) \\
& \geq \;\; \sum_{k=2}^{K} \frac{|\mathcal{S}_k|}{|\mathcal{S}|} \frac{C_4 L_k \rho_N^2}{N(N-1)} \| \widehat{\boldsymbol{D}} - \boldsymbol{D}^\star \|_F^2.
\end{aligned}$$

Since $(\widehat{\boldsymbol{D}}, \widehat{\boldsymbol{\alpha}})$ maximizes the loglikelihood, i.e., $\sum_{e \in \mathcal{S}} \big(\ell(\widehat{\boldsymbol{D}}, \widehat{\boldsymbol{\alpha}}) - \ell(\boldsymbol{D}^\star, \boldsymbol{\alpha}^\star) \big) \geq 0$, we get for Equation (A.4)

$$\begin{aligned}
& \sup_{\boldsymbol{D}, \boldsymbol{\alpha}} \left| \frac{1}{|\mathcal{S}|} \sum_{e \in \mathcal{S}_k} \ell(Z_e \mid \boldsymbol{D}, \boldsymbol{\alpha}) - \mathbb{E}\, \ell(Z_e \mid \boldsymbol{D}, \boldsymbol{\alpha}) \right| \\
& \geq \;\; - \sum_{k=2}^{K} \frac{1}{|\mathcal{S}|} \sum_{e \in \mathcal{S}_k} \mathbb{E}\, \ell_k(Z_e \mid \widehat{\boldsymbol{D}}, \widehat{\alpha}_k) - \mathbb{E}\, \ell_k(Z_e \mid \boldsymbol{D}^\star, \alpha_k^\star) \\
& \geq \;\; \sum_{k=2}^{K} \frac{C_4 |\mathcal{S}_k|\, L_k\, \rho_N^2}{|\mathcal{S}|\, N\, (N-1)} \| \boldsymbol{D} - \boldsymbol{D}^\star \|_F^2.
\end{aligned} \tag{A.11}$$

Next, we bound the empirical process $\sup_{\boldsymbol{D}, \boldsymbol{\alpha}} |1/|\mathcal{S}| \sum_{e \in \mathcal{S}_k} \ell(Z_e \mid \boldsymbol{D}, \boldsymbol{\alpha}) - \mathbb{E}\, \ell(Z_e \mid \boldsymbol{D}, \boldsymbol{\alpha})|$ with high probability. Based on Condition 2 and 3, we define the parameter space for latent positions by

$$\boldsymbol{\Phi} \;\; := \;\; \{ \boldsymbol{\Theta} \in \mathbb{R}^+ \times \mathbb{R}^r \mid -C_2 \leq \boldsymbol{\Theta}_{i,j} \leq C_2, j = 2, \ldots, r+1 \},$$

and the parameter space for hyperbolic Gram matrix $\boldsymbol{D}$ by

$$\boldsymbol{\Omega} \;\coloneqq\; \{\boldsymbol{\Theta}\boldsymbol{J}\boldsymbol{\Theta}^\top \mid \boldsymbol{\Theta} \in \mathbb{R}^+ \times \mathbb{R}^r,\; -C_2 \le \boldsymbol{\Theta}_{i,j} \le C_2, j = 2, \ldots, r+1,\; D_{i,j} \ge C_3\}.$$

We introduce the δ-covering number of a metric space $(\boldsymbol{X},\, d)$ as

$$N(\delta,\, \boldsymbol{X},\, d) \coloneqq \inf\{N \in \mathcal{N} : \exists \text{ a } \delta\text{-covering } x_1, \ldots, x_N \text{ of } \boldsymbol{X}\}.$$

In this context, the set $\{a_1, ..., a_k\}$ for some $M \in \{1, 2, ...\}$ is a δ-covering of X if there exists some $k = 1, ..., M$ for any $x \in X$ such that $d(x, a_k) \le \epsilon$. Then we have $N(\delta,\, \boldsymbol{\Phi},\, \|\cdot\|_\infty) \le (1 + C_2/\delta)^{Nr}$, where $\|\cdot\|_\infty$ denotes the ℓ_∞-norm. Then, for any $\boldsymbol{D} = \boldsymbol{\Theta}\,\boldsymbol{J}\,\boldsymbol{\Theta}^\top \in \boldsymbol{\Omega}$, we can find $\widetilde{\boldsymbol{\Theta}} \in \boldsymbol{\Phi}$ such that $\|\boldsymbol{\Theta} - \widetilde{\boldsymbol{\Theta}}\|_\infty \le \delta$, and

$$\|\boldsymbol{D} - \widetilde{\boldsymbol{D}}\|_\infty \;=\; \|\boldsymbol{\Theta}\,\boldsymbol{J}\,\boldsymbol{\Theta}^\top - \widetilde{\boldsymbol{\Theta}}\,\boldsymbol{J}\,\widetilde{\boldsymbol{\Theta}}^\top\|_\infty \;\le\; 2\,\|\widetilde{\boldsymbol{\Theta}}\,\boldsymbol{J}\,(\boldsymbol{\Theta} - \widetilde{\boldsymbol{\Theta}})\|_\infty \;\le\; 6\,C_2\,\delta.$$

Therefore, we obtain

$$\begin{aligned} N(6\,C_2\,\delta,\, \boldsymbol{\Omega},\, \|\cdot\|_\infty) &\le N(\delta,\, \boldsymbol{\Phi},\, \|\cdot\|_\infty) \\ N(\delta,\, \boldsymbol{\Omega},\, \|\cdot\|_\infty) &\le \left(1 + \frac{6\,C_2^2}{\delta}\right)^{N\,r}. \end{aligned}$$

Now we introduce the element-wise loss function for a size-k hyperedge $e = (i_1, \ldots, i_k)$ as

$$\ell_k(e) \;=\; \mathbf{1}_{\{e \in \mathcal{S}_k\}}\big(Z_e \log \alpha_k f_k^{(e)}(\boldsymbol{D}) + (1 - Z_e)\log(1 - \alpha_k f_k^{(e)}(\boldsymbol{D}))\big),$$

where $\mathbf{1}_{\{\cdot\}}$ is the indicator random variable, and is 1 for $e \in \mathcal{S}_k$. With the function space $\boldsymbol{L}_k \coloneqq \{\ell_k(Z_e \mid \alpha_k, \boldsymbol{D}),\; \alpha_k \in [C_1, 1],\; \boldsymbol{D} \in \boldsymbol{\Omega}\}$, we get for any $\boldsymbol{D}, \widetilde{\boldsymbol{D}} \in \boldsymbol{\Omega}$ and any

$\alpha_k, \widetilde{\alpha}_k \in [C_1, 1]$:

$$
\begin{aligned}
& |\ell_k(Z_e \mid \alpha_k, \boldsymbol{D}) - \ell_k(Z_e \mid \widetilde{\alpha}_k, \widetilde{\boldsymbol{D}})| \\
= & \left| \mathbf{1}_{\{(i_1,\ldots,i_k)\}} \left(Z_e \log \frac{\alpha_k f_k^{(e)}(\boldsymbol{D})}{\widetilde{\alpha}_k f_k^{(e)}(\widetilde{\boldsymbol{D}})} + (1 - Z_e) \log \frac{1 - \alpha_k f_k^{(e)}(\boldsymbol{D})}{1 - \widetilde{\alpha}_k f_k^{(e)}(\widetilde{\boldsymbol{D}})} \right) \right| \\
\leq & |\mathbf{1}_{\{(i_1,\ldots,i_k)\}}| \\
\times & \left| \frac{A_k^e}{f_k^{(e)}(\boldsymbol{\epsilon})(1 - f_k^{(e)}(\boldsymbol{\epsilon}))} \sum_{(i,j)\subset e} \frac{\partial f_k^{(e)}(\boldsymbol{\epsilon})}{\partial \boldsymbol{D}_{i,j}} (\boldsymbol{D}_{i,j} - \widetilde{D}_{i,j}) + \frac{A_k^e}{\alpha(1 - \alpha f_k^{(e)}(\boldsymbol{\epsilon}))} (\alpha_k - \widetilde{\alpha}_k) \right| \\
\leq & |\mathbf{1}_{\{(i_1,\ldots,i_k)\}}| \left(\sum_{(i,j)\subset e} \frac{1}{f_k^{(e)}(\boldsymbol{\epsilon})(1 - f_k^{(e)}(\boldsymbol{\epsilon}))} \left| \frac{\partial f_k^{(e)}(\boldsymbol{\epsilon})}{\partial \boldsymbol{D}_{i,j}} \right| |\boldsymbol{D}_{i,j} - \widetilde{D}_{i,j}| \right. \\
+ & \left. \frac{1}{\alpha(1 - \alpha f_k^{(e)})(\boldsymbol{\epsilon})} |\alpha_k - \widetilde{\alpha}_k| \right) \\
\leq & \max \left(\left| \frac{\partial f_k^{(e)}(\boldsymbol{\epsilon})}{f_k^{(e)}(\boldsymbol{\epsilon})(1 - f_k^{(e)}(\boldsymbol{\epsilon}))\, \partial \boldsymbol{D}_{i,j}} \right|, \frac{1}{\alpha(1 - \alpha f_k^{(e)}(\boldsymbol{\epsilon}))} \right) (k+1) \\
\times & \max(\|\boldsymbol{D} - \widetilde{\boldsymbol{D}}\|_\infty, |\alpha_k - \widetilde{\alpha}_k|),
\end{aligned}
$$

where $A_k^e = Z_e(1 - \alpha f_k^{(e)}(\boldsymbol{\epsilon})) + (1 - Z_e)(-\alpha f_k^{(e)}(\boldsymbol{\epsilon}))$, and $\alpha \in (\alpha_k, \widetilde{\alpha}_k)$ and $\boldsymbol{\epsilon} = \{\epsilon_{i,j}\}$, $\epsilon_{i,j} \in (\boldsymbol{D}_{i,j}, \widetilde{D}_{i,j})$. Based on Conditions 1, 2 and 3, there exist constants $C(C_1, C_2, C_3) > 0$ and $C'(C_1, C_2, C_3) > 0$ where C and C' are functions of C_1, C_2, C_3 such that

$$
\begin{aligned}
\left| \frac{1}{f_k^{(e)}(\boldsymbol{\epsilon})(1 - f_k^{(e)}(\boldsymbol{\epsilon}))} \frac{\partial f_k^{(e)}(\boldsymbol{\epsilon})}{\partial \boldsymbol{D}_{i,j}} \right| & \leq \max_{i \in e} \left(\sum_{j \in e} \boldsymbol{\epsilon}_{i,j} \right) \left(\frac{1}{\sum_{j \in e} \boldsymbol{\epsilon}_{i,j}} + \frac{1}{\sum_{k \in e} \boldsymbol{\epsilon}_{jk}} \right) \frac{1}{\sqrt{\boldsymbol{\epsilon}_{i,j}^2 - 1}} \\
& \leq C \\
\frac{1}{\alpha(1 - \alpha f_k^{(e)}(\boldsymbol{\epsilon}))} & \leq C'.
\end{aligned}
$$

Therefore, we have with $C_0 \coloneqq \max(C, C')$:

$$
|\ell_k(Z_e \mid \alpha_k, \boldsymbol{D}) - \ell_k(Z_e \mid \widetilde{\alpha}_k, \widetilde{\boldsymbol{D}})| \leq C_0(k+1) \max(\|\boldsymbol{D} - \widetilde{\boldsymbol{D}}\|_\infty, |\alpha_k - \widetilde{\alpha}_k|). \tag{A.12}
$$

In the following, we consider the function space $(\boldsymbol{L}_k, d_{\boldsymbol{L}_k})$ defined above with the metric as $d_{\boldsymbol{L}_k}((\boldsymbol{D}, \alpha_k), (\widetilde{\boldsymbol{D}}, \widetilde{\alpha}_k)) := \max(\|\boldsymbol{D} - \widetilde{\boldsymbol{D}}\|_\infty, |\alpha_k - \widetilde{\alpha}_k|)$. Based on Lemma 2.14 in Sen

(2018), the bracketing number $N_{[\,]}(2\delta\|l_{\max}\|_F, \boldsymbol{L}_k, \|\cdot\|_F) \leq N(\delta, [C_1, 1] \otimes \boldsymbol{\Omega}, d_{\boldsymbol{L}_k})$ where $l_{\max} = C_0(k+1)$, and $\otimes$ denotes the Cartesian product between two spaces.

$$
\begin{aligned}
& N(\delta,\, [C_1,\, 1] \otimes \boldsymbol{\Omega},\, d_{\boldsymbol{L}_k}) \\
\leq\;& N(\delta,\, \boldsymbol{\Omega},\, \|\cdot\|_\infty)\, N(\delta,\, [C_1,\, 1], |\cdot|) \\
\leq\;& \left(1 + \frac{6\, C_2^2}{\delta}\right)^{N\, r} \left(1 + \frac{1 - C_1}{\delta}\right) \\
\leq\;& \left(1 + \frac{\max(6\, C_2^2, 1 - C_1)}{\delta}\right)^{N\, r+1},
\end{aligned}
$$

which yields

$$
N_{[\,]}(\delta,\, \boldsymbol{L}_k,\, \|\cdot\|_F) \;\leq\; \left(1 + \frac{2\, C_0\, (k+1) \max(6\, C_2^2,\, 1 - C_1)}{\delta}\right)^{N\, r+1}.
$$

Notice that the above argument holds for $k \in \{2, \ldots, K\}$, which implies the following result for the loglikelihood function:

$$
\begin{aligned}
\left|\ell(Z_e \mid \boldsymbol{D}, \boldsymbol{\alpha}_k) - \ell(Z_e \mid \widetilde{\boldsymbol{D}}, \widetilde{\boldsymbol{\alpha}}_k)\right| \;&\leq\; \sum_{k=2}^{K} \left|\ell_k(Z_e \mid \boldsymbol{D}, \boldsymbol{\alpha}_k) - \ell_k(Z_e \mid \widetilde{\boldsymbol{D}}, \widetilde{\boldsymbol{\alpha}}_k\right| \\
&\leq\; C_0 \sum_{k=2}^{K} (k+1)\, \max(\|\boldsymbol{D} - \widetilde{\boldsymbol{D}}\|_\infty, \|\boldsymbol{\alpha} - \widetilde{\boldsymbol{\alpha}}\|_\infty)
\end{aligned}
$$

Similarly, we consider the function space $(\boldsymbol{L}, d_{\boldsymbol{L}})$ with

$$
\boldsymbol{L} \;\coloneqq\; \left\{\ell(\cdot \mid \boldsymbol{D}, \boldsymbol{\alpha}),\; \boldsymbol{\alpha} \in [C_1, 1]^{K-1},\; \boldsymbol{D} \in \boldsymbol{\Omega}\right\}
$$

and metric as $d_{\boldsymbol{L}}((\widetilde{\boldsymbol{D}}, \widetilde{\boldsymbol{\alpha}}), (\boldsymbol{D}, \boldsymbol{\alpha})) := \max(\|\boldsymbol{D} - \widetilde{\boldsymbol{D}}\|_\infty, \|\boldsymbol{\alpha} - \widetilde{\boldsymbol{\alpha}}\|_\infty)$. In that context, we get

$$
\begin{aligned}
N(\delta, [C_1, 1]^{K-1} \otimes \boldsymbol{\Omega}, d_{\boldsymbol{L}}) \;&\leq\; N(\delta, \boldsymbol{\Omega}, \|\cdot\|_\infty)\, N(\delta, [C_1, 1]^{K-1}, \|\cdot\|_\infty) \\
&\leq\; \left(1 + \frac{\max(6\, C_2^2, 1 - C_1)}{\delta}\right)^{Nr+K-1},
\end{aligned}
$$

and $N_{[\,]}(2\delta\|l_{\max}\|_F, \boldsymbol{L}, \|\cdot\|_F) \leq N(\delta, [C_1, 1]^{K-1} \otimes \boldsymbol{\Omega}, d_{\boldsymbol{L}})$ where $l_{\max} = C_0 \sum_{k=2}^{K}(k+1)$. Then we have

$$
N_{[\,]}(\delta, \boldsymbol{L}, \|\cdot\|_F) \;\leq\; \left(1 + \frac{C_0(K+4)(K-1) \max(6C_2^2, 1 - C_1)}{\delta}\right)^{Nr+K-1}.
$$

Then, from Theorem 4.12 in Sen (2018),

$$\begin{aligned} & \mathbb{E} \sup_{\boldsymbol{D}\in\boldsymbol{\Omega},\,\boldsymbol{\alpha}\in[C_1,1]^{K-1}} \left| \frac{1}{|\mathcal{S}|} \sum_{e\in\mathcal{S}_k} \ell(Z_e \mid \boldsymbol{D},\boldsymbol{\alpha}) - \mathbb{E}\,\ell(Z_e \mid \boldsymbol{D},\boldsymbol{\alpha}) \right| \\ \leq & \frac{\int_0^{C_{\max}} \sqrt{\log N_{[\,]}(\delta,\boldsymbol{L},\|\cdot\|_F)}\boldsymbol{d}\delta}{\sqrt{|\mathcal{S}|}} \\ \leq & \frac{C_0\sqrt{(N\,r+K-1)\,(K+4)\,(K+1)}}{\sqrt{|\mathcal{S}|}}, \end{aligned} \tag{A.13}$$

where $C_{\max} := \|\sup_{l\in\boldsymbol{L}} \ell(Z_e)\|_F$ is independent of N and $|\mathcal{S}|$, and $C := 2\sqrt{2\,C_{\max}\,C_0\,\max(6\,C_2^2,\,1-C_1)}$. Then, by combining (A.11) and (A.13), and using Markov inequality we have with probability at least $1-\epsilon$:

$$\frac{1}{N(N-1)}\|\widehat{\boldsymbol{D}}-\boldsymbol{D}\|_F^2 \;\leq\; C\left(\sum_{k=2}^{K}\frac{C_4\,|\mathcal{S}_k|\,L_k}{|\mathcal{S}|}\right)^{-1}\frac{\sqrt{(Nr+K-1)\,(K+4)\,(K+1)}}{\epsilon\,\rho_N^2\,\sqrt{|\mathcal{S}|}},$$

where $C>0$ is a constant.

Last, but not least, we establish non-asymptotic error bounds on estimators of $\boldsymbol{\alpha}$. By Equation (A.11), we have

$$\sup_{\boldsymbol{D},\boldsymbol{\alpha}}\left|\frac{1}{|\mathcal{S}|}\sum_{e\in\mathcal{S}_k}\ell(Z_e\mid\boldsymbol{D},\boldsymbol{\alpha})-\mathbb{E}\,\ell(Z_e\mid\boldsymbol{D},\boldsymbol{\alpha})\right| \;\geq\; \frac{L_k|\mathcal{S}_k|}{|\mathcal{S}|}D_k(\boldsymbol{P}_k^\star\|\widehat{\boldsymbol{P}}_k).$$

Also from Equation (A.7), we have $\boldsymbol{D}_k^{(2)}(\boldsymbol{P}_k^\star,\widehat{\boldsymbol{P}}_k,\boldsymbol{Q}_k)\leq\max(1,|1-\rho_N^{-1}|)D_k(\boldsymbol{P}_k^\star\|\widehat{\boldsymbol{P}}_k)$. Then, by similarly using (A.13) and the Markov inequality, we have with probability at least $1-\epsilon$:

$$\boldsymbol{D}_k^{(2)}(\boldsymbol{P}_k^\star,\widehat{\boldsymbol{P}}_k,\boldsymbol{Q}_k) \;\leq\; C\,\frac{|\mathcal{S}|\,\sqrt{(N\,r+K-1)\,(K+4)\,(K+1)}}{\epsilon\,\rho_N\,L_k\,\sqrt{|\mathcal{S}|}\,|\mathcal{S}_k|}.$$

Finally, by defining $h(x) := a\log\frac{b}{x}+(1-a)\log\frac{1-b}{x}$ with $a=\alpha_k^\star\,f_k^{(e)}(\boldsymbol{D}^\star)$ and $b=\alpha_k^\star\,f_k^{(e)}(\widehat{\boldsymbol{D}})$, we use a first-order Taylor expansion for $x=\widehat{\alpha}_k\,f_k^{(e)}(\widehat{\boldsymbol{D}})$ at b, we obtain

$$\boldsymbol{D}_k^{(2)}(\boldsymbol{P}_k^\star,\widehat{\boldsymbol{P}}_k,\boldsymbol{Q}_k) \;\geq\; C_5\,|\widehat{\alpha}_k-\alpha_k|,$$

where C_5 is independent of N and $|\mathcal{S}|$ based on Conditions 1 and 3.

A.3 Proof of Theorem 2

Theorem 2 *Under Conditions 1–5, assuming that N and $|\mathcal{S}|$ increase without bound,*

$$\frac{1}{N}\inf_{\boldsymbol{R}\in\mathcal{R}}\|\widehat{\boldsymbol{\Theta}}\,\boldsymbol{R}-\boldsymbol{\Theta}^{\star}\|_F^2 \;=\; O_p\left(\frac{\Delta_{N,2}}{\rho_N^2\sqrt{|\mathcal{S}|}}\right),$$

where $\mathcal{R}:=\{\boldsymbol{R}\in\mathbb{R}^{3\times 3}:\ \boldsymbol{R}\,\boldsymbol{J}\,\boldsymbol{R}^{\top}=\boldsymbol{J}\}$ is the set of hyperbolic rotation matrices.

According to Theorem 1, we know that $\|\widehat{\boldsymbol{D}}-\boldsymbol{D}^{\star}\|_F^2 = O_p(N^2/(\rho_N^2 M))$, where $M = \sqrt{|\mathcal{S}|}/\Delta_{N,2}$ when $r=2$. We perform a singular value decomposition (SVD) of $\boldsymbol{D}=\boldsymbol{U}\boldsymbol{S}\boldsymbol{U}^{\top}$, with a matrix consisting of the left singular vectors $\boldsymbol{U}\in\mathbb{R}^{N\times 3}$ and the diagonal matrix of all singular values $\boldsymbol{S}=\mathrm{diag}(s_1,s_2,s_3)\in\mathbb{R}^{3\times 3}$, and denote its estimator by $\widehat{\boldsymbol{D}}=\widehat{\boldsymbol{U}}\widehat{\boldsymbol{S}}\widehat{\boldsymbol{U}}^{\top}$. Based on Tabaghi and Dokmanić (2020), we can arrange eigenvalues as $s_1<0<s_2<s_3$. Define the operator norm induced by a vector norm $\|\cdot\|$ by $\|\boldsymbol{A}\|_{op}=\sup_{\|\mathbf{x}\|=1}\|\boldsymbol{A}\mathbf{x}\|$, where the supremum is taken over all non-zero vectors $\mathbf{x}\in\mathbb{R}^n$, and $\|\cdot\|$ denotes the vector l_2 norm. Given that $\|\boldsymbol{D}\|_{op}\le\|\boldsymbol{D}\|_F\asymp N$ and Condition 4 hold, we have $|s_i|\asymp N,\ i=1,2,3$. Therefore, $|\widehat{s}_i|\asymp N\ (i=1,2,3)$ by Tang and Priebe (2018).

In the following, we establish the result for $\widetilde{\boldsymbol{\Theta}}:=\boldsymbol{U}\,|\boldsymbol{S}|^{1/2}\boldsymbol{J}$ relying on Theorem 3 in Rubin-Delanchy et al. (2022). We follow the proof of Theorem 3 in Rubin-Delanchy et al. (2022) by $\boldsymbol{D}$ and $\widehat{\boldsymbol{D}}$. We split the columns of $\boldsymbol{U}=\left[\boldsymbol{U}_{(-)}\mid\boldsymbol{U}_{(+)}\right]$ where $\boldsymbol{U}_{(-)}$ and $\boldsymbol{U}_{(+)}$ are eigenvectors corresponding to negative and positive eigenvalues, respectively. We use same notations for $\widehat{\boldsymbol{U}}$. We check and decompose the matrix $\boldsymbol{U}^{\top}\widehat{\boldsymbol{U}}$ as

$$\boldsymbol{U}^{\top}\hat{\boldsymbol{U}} \;=\; \left[\begin{array}{c|c} \boldsymbol{U}_{(-)}^{\top}\hat{\boldsymbol{U}}_{(-)} & \boldsymbol{U}_{(-)}^{\top}\hat{\boldsymbol{U}}_{(+)} \\ \hline \boldsymbol{U}_{(+)}^{+}\boldsymbol{U}_{(-)} & \boldsymbol{U}_{(+)}^{\top}\hat{\boldsymbol{U}}_{(+)} \end{array}\right]\in\mathbb{R}^{3\times 3}$$

We perform a singular value decomposition on $\boldsymbol{U}_{(+)}^{\top}\hat{\boldsymbol{U}}_{(+)}=\mathbf{W}_{(+),1}\boldsymbol{\Sigma}_{(+)}\mathbf{W}_{(+),2}^{\top}$ and $\boldsymbol{U}_{(-)}^{\top}\hat{\boldsymbol{U}}_{(-)}=\mathbf{W}_{(-),1}\boldsymbol{\Sigma}_{(-)}\mathbf{W}_{(-),2}^{\top}$. And we define matrix $\boldsymbol{W}$ as

$$\boldsymbol{W} \;=\; \left[\begin{array}{c|c} \mathbf{w}_{(-)}^{*} & \mathbf{0} \\ \hline \mathbf{0} & \mathbf{w}_{(+)}^{*} \end{array}\right]\in\mathbb{R}^{3\times 3},$$

where $\boldsymbol{W}^*_{(+)} = \mathbf{W}_{(+),1}\mathbf{W}^\top_{(+),2}$ and $\boldsymbol{W}^*_{(-)} = \mathbf{W}_{(-),1}\mathbf{W}^\top_{(-),2}$. Notice that $\mathbf{W}$ is an orthogonal matrix and $\boldsymbol{W}\boldsymbol{J}\boldsymbol{W}^\top = \boldsymbol{J}$. In the following, we show that $\boldsymbol{U}^\top\widehat{\boldsymbol{U}}$ is close to $\boldsymbol{W}$. First, we have

$$\|\boldsymbol{U}^\top_{(+)}\hat{\boldsymbol{U}}_{(+)} - \mathbf{W}^\star_{(+)}\|_F \;=\; \|\boldsymbol{\Sigma}_{(+)} - \mathbf{I}\|_F \;\leq\; \|\boldsymbol{U}_{(+)}\boldsymbol{U}^\top_{(+)} - \hat{\boldsymbol{U}}_{(+)}\hat{\boldsymbol{U}}^\top_{(+)}\|^2_F.$$

Upon invoking the Davis-Kahan theorem, we obtain

$$\|\boldsymbol{U}^\top_{(+)}\hat{\boldsymbol{U}}_{(+)} - \mathbf{W}^\star_{(+)}\|_F \;\leq\; \|\boldsymbol{U}_{(+)}\boldsymbol{U}^\top_{(+)} - \hat{\boldsymbol{U}}_{(+)}\hat{\boldsymbol{U}}^\top_{(+)}\|^2_F \;=\; O_p\left(\frac{\|\boldsymbol{D} - \widehat{\boldsymbol{D}}\|^2}{s^2_{\min}(\boldsymbol{D})}\right),$$

where $s_{\min}(\boldsymbol{D})$ is the smallest eigenvalue of $\boldsymbol{D}$ in magnitude. Based on Condition 4, we have $s_{\min}(\boldsymbol{D}) \asymp N$, hence

$$\|\boldsymbol{U}^\top_{(+)}\widehat{\boldsymbol{U}}_{(+)} - \boldsymbol{W}^\star_{(+)}\|_F \;=\; O_p\left(\frac{1}{\rho^2_N\, M}\right).$$

We have same result for $\|\boldsymbol{U}^\top_{(-)}\widehat{\boldsymbol{U}}_{(-)} - \boldsymbol{W}^\star_{(-)}\|_F = O_p\left(1/(\rho^2_N\, M)\right)$. Next we bound $\|\boldsymbol{U}^\top_{(+)}\widehat{\boldsymbol{U}}_{(-)}\|_F$, i.e., we bound each (i,j) element in $\boldsymbol{U}^\top_{(+)}\widehat{\boldsymbol{U}}_{(-)}$ for $i = 1,2$ and $j = 1$. We denote the i-th column of $\boldsymbol{U}_{(+)}$ as $\boldsymbol{u}_i$ and the corresponding eigenvalues are s_{i+1} for $i = 1,2$. Then

$$\begin{aligned}
(\boldsymbol{U}^\top_{(+)}\widehat{\boldsymbol{U}}_{(-)})_{i,1} &= (\hat{s}_1 - s_{i+1})^{-1}\,(\boldsymbol{u}_i)^\top\,(\widehat{\boldsymbol{D}} - \boldsymbol{D})\widehat{\boldsymbol{U}}_{(-)} \\
&= (\hat{s}_1 - s_{i+1})^{-1}\,(\boldsymbol{u}_i)^\top\,(\widehat{\boldsymbol{D}} - \boldsymbol{D})\boldsymbol{U}_{(-)}\boldsymbol{U}^\top_{(-)}\widehat{\boldsymbol{U}}_{(-)} \\
&+ (\hat{s}_1 - s_{i+1})^{-1}\,(\boldsymbol{u}_i)^\top\,(\widehat{\boldsymbol{D}} - \boldsymbol{D})\left(\mathbf{I} - \boldsymbol{U}_{(-)}\boldsymbol{U}^\top_{(-)}\right)\widehat{\boldsymbol{U}}_{(-)}.
\end{aligned}$$

We first consider term $\boldsymbol{u}_i^\top(\widehat{\boldsymbol{D}} - \boldsymbol{D})\,\boldsymbol{U}_{(-)} \in \mathbb{R}$

$$\begin{aligned}
\|\boldsymbol{u}_i^\top(\widehat{\boldsymbol{D}} - \boldsymbol{D})\,\boldsymbol{U}_{(-)}\|_F &= \text{trace}\left((\widehat{\boldsymbol{D}} - \boldsymbol{D})\,\boldsymbol{U}_{(-)}\,\boldsymbol{u}_i^\top\right) \\
&\leq \|\widehat{\boldsymbol{D}} - \boldsymbol{D}\|_{op}\,\|\boldsymbol{U}_{(-)}\,\boldsymbol{u}_i^\top\|_{op} \\
&= O_p\left(\frac{N}{\sqrt{\rho^2_N M}}\right),
\end{aligned}$$

where we use $\|\widehat{\boldsymbol{D}} - \boldsymbol{D}\|_{op} \leq \|\widehat{\boldsymbol{D}} - \boldsymbol{D}\|_F \asymp N/(\rho^2_N M)^{1/2}$ based on the von Neumann trace inequality along with $\|\boldsymbol{U}_{(-)}\,\boldsymbol{u}_i^\top\|_{\text{op}} = 1$. In addition, using the fact that $\hat{s}_i, s_i \asymp N$ $(i = 1,2,3)$, we obtain

$$\|\,(\hat{s}_1 - s_{i+1})^{-1}\,(\boldsymbol{u}_i)^\top\,(\widehat{\boldsymbol{D}} - \boldsymbol{D})\boldsymbol{U}_{(-)}\boldsymbol{U}^\top_{(-)}\widehat{\boldsymbol{U}}_{(-)}\|_F \;=\; O_p\left(\frac{1}{\sqrt{\rho^2_N\, M}}\right)$$

We notice that

$$\|\boldsymbol{u}_i^\top(\widehat{\boldsymbol{D}}-\boldsymbol{D})\|_F \;\leq\; \|\widehat{\boldsymbol{D}}-\boldsymbol{D}\|_{\text{op}} \;=\; O_p\left(\frac{N}{\sqrt{\rho_N^2\,M}}\right),$$

and, according to the Davis-Kahan theorem,

$$\begin{aligned}\left\|\left(\mathbf{I}-\boldsymbol{U}_{(-)}\boldsymbol{U}_{(-)}^\top\right)\widehat{\boldsymbol{U}}_{(-)}\right\|_F &= \|(\mathbf{I}-\boldsymbol{U}_{(-)}\boldsymbol{U}_{(-)}^\top)\widehat{\boldsymbol{U}}_{(-)}\widehat{\boldsymbol{U}}_{(-)}^\top\|_F \;\leq\; \|\boldsymbol{U}_{(-)}\boldsymbol{U}_{(-)}^\top-\widehat{\boldsymbol{U}}_{(-)}\widehat{\boldsymbol{U}}_{(-)}^\top\|_F\\ &= O_p\left(\frac{\|\boldsymbol{D}-\widehat{\boldsymbol{D}}\|^2}{s_{\min}^2(\boldsymbol{D})}\right)\\ &= O_p\left(\frac{1}{\rho_N^2\,M}\right).\end{aligned}$$

Then we have

$$\|(\hat{s}_1-s_{i+1})^{-1}\left(\boldsymbol{u}_i\right)^\top\left(\widehat{\boldsymbol{D}}-\boldsymbol{D}\right)\left(\mathbf{I}-\boldsymbol{U}_{(-)}\boldsymbol{U}_{(-)}^\top\right)\widehat{\boldsymbol{U}}_{(-)}\|_F \;=\; O_p\left(\frac{1}{(\rho_N^2\,M)^{3/2}}\right).$$

Thus we have $\|\boldsymbol{U}_{(+)}^\top\widehat{\boldsymbol{U}}_{(-)})\|_F = O_p(1/\sqrt{\rho_N^2\,M})$. Upon combining the results on the diagnoal block, we obtain

$$\|\boldsymbol{U}^\top\widehat{\boldsymbol{U}}-\boldsymbol{W}\|_F \;=\; O_p\left(\frac{1}{\sqrt{\rho_N^2\,M}}\right).$$

Given the matrix equation $\hat{\boldsymbol{U}}\hat{\boldsymbol{S}}-(\widehat{\boldsymbol{D}}-\boldsymbol{D})\hat{\boldsymbol{U}}=\boldsymbol{D}\hat{\boldsymbol{U}}$, we have the matrix series expansion following proof of Theorem 3 in Supplement C.2 of Rubin-Delanchy et al. (2022). Specifically, we place $A-P$ as $\widehat{\mathbf{D}}-\mathbf{D}$, and obtain

$$\begin{aligned}\hat{\mathbf{U}}|\hat{\mathbf{S}}|^{1/2} &= \sum_{k=0}^{\infty}(\widehat{\mathbf{D}}-\mathbf{D})^k\mathbf{U}\mathbf{S}\mathbf{U}^\top\hat{\mathbf{U}}\mathbf{J}^{k+1}|\hat{\mathbf{S}}|^{-k-1/2}\\ &= \mathbf{U}|\mathbf{S}|^{1/2}\boldsymbol{W}+(\widehat{\mathbf{D}}-\mathbf{D})\mathbf{U}|\mathbf{S}|^{-1/2}\mathbf{W}\mathbf{J}+\underbrace{\sum_{k=2}^{\infty}(\widehat{\mathbf{D}}-\mathbf{D})^k\mathbf{U}|\mathbf{S}|^{-k+1/2}\mathbf{W}\mathbf{J}^{k+2}}_{\boldsymbol{R}_{V_1}}\\ &+ \underbrace{\sum_{k=0}^{\infty}(\widehat{\mathbf{D}}-\mathbf{D})^k\mathbf{U}\mathbf{J}|\mathbf{S}|^{-k+1/2}\left(\mathbf{U}^\top\hat{\mathbf{U}}-\mathbf{W}\right)\mathbf{J}^{k+1}}_{V_2}\\ &+ \underbrace{\sum_{k=0}^{\infty}(\widehat{\mathbf{D}}-\mathbf{D})^k\mathbf{U}\mathbf{S}\left(\mathbf{U}^\top\hat{\mathbf{U}}\mathbf{J}^{k+1}|\hat{\mathbf{S}}|^{-k-1/2}-|\mathbf{S}|^{-k-1/2}\mathbf{U}^\top\hat{\mathbf{U}}\mathbf{J}^{k+1}\right)}_{V_3}\end{aligned}$$

Following Lemma 12 in Rubin-Delanchy et al. (2022), we have the following expansion:

$$\hat{\mathbf{U}}|\hat{\mathbf{S}}|^{1/2} \;=\; \mathbf{U}|\mathbf{S}|^{1/2}\,\boldsymbol{W}+(\widehat{\boldsymbol{D}}-\boldsymbol{D})\,\boldsymbol{U}\,|\boldsymbol{S}|^{-1/2}\,\boldsymbol{W}\,\boldsymbol{J}+\boldsymbol{R}_{V_1}+\boldsymbol{V}_2+\boldsymbol{V}_3. \tag{A.14}$$

We estimate the order of all terms on the left hand side except $\mathbf{U}|\mathbf{S}|^{1/2}\boldsymbol{W}$ following the proof in C.2 of Theorem 3. Specifically, we replace $\|\cdot\|_{2\to\infty}$ by $\|\cdot\|_F$ using the fact that for any matrix $\boldsymbol{A}\in\mathbb{R}^{n\times n}$, $\|\boldsymbol{A}\|_F \le \sqrt{\text{rank}(\boldsymbol{A})}\,\|\boldsymbol{A}\|_{op} \le \sqrt{\text{rank}(\boldsymbol{A})\,n}\|\boldsymbol{A}\|_{2\to\infty}$.

We obtain the asymptotic order of four above residual terms similar to the argument in sections (C.2.1), (C.2.2), and (C.2.3) of the proof for Theorem 3 from Rubin-Delanchy et al. (2022). First, given $\text{rank}(\widehat{\boldsymbol{D}}-\boldsymbol{D})=O(1)$ and the submultiplication of $\|\cdot\|_F$, we have

$$\|(\widehat{\boldsymbol{D}}-\boldsymbol{D})\,\boldsymbol{U}|\boldsymbol{S}|^{-1/2}\,\boldsymbol{W}\,\boldsymbol{J}\|_F = O_p((N/(\rho_N^2 M)^{1/2})\,N^{-1/2}) = O_p((N/(\rho_N^2 M))^{1/2}).$$

With regard to $\boldsymbol{R}_{V_1}$, notice that $\|\boldsymbol{U}\|_F$, $\|\boldsymbol{W}\|_F$, $\|\boldsymbol{J}\|_F = O(1)$ and $M>1$, we have

$$\begin{aligned}\|\boldsymbol{R}_{V_1}\|_F &\le \sum_{k=2}^{\infty} O_p(\|\widehat{\boldsymbol{D}}-\boldsymbol{D}\|_F^k\||\boldsymbol{S}|\|_F^{-k+1/2}) \le \sum_{k=2}^{\infty} O_p((N/(\rho_N^2 M)^{1/2})^k N^{-k+1/2}) \\ &= O_p\left(\frac{N^{1/2}}{\rho_N^2\,M}\right).\end{aligned}$$

With regard to $\boldsymbol{V}_2$, following the argument in C.2.2, we have

$$\begin{aligned}\|\boldsymbol{V}_2\|_F &\le \||\mathbf{S}|\|_F^{1/2}\|\mathbf{U}^\top\hat{\mathbf{U}}-\mathbf{W}\|_F + \|\widehat{\mathbf{D}}-\mathbf{D}\|_F\|\mathbf{S}|\|_F^{-1/2}\|\mathbf{U}^\top\hat{\mathbf{U}}-\mathbf{W}\|_F + o_p(\|\boldsymbol{R}_{V_1}\|_F) \\ &= O_p\left(N^{1/2}\times\frac{1}{(\rho_N^2 M)^{1/2}}\right) + O_p\left(\frac{N}{(\rho_N^2 M)^{1/2}}\times\frac{1}{N^{1/2}}\times\frac{1}{(\rho_N^2 M)^{1/2}}\right) \\ &= O_p\left((\frac{N}{\rho_N^2 M})^{1/2} + \frac{N^{1/2}}{\rho_N^2 M}\right)\end{aligned}$$

With regard to $\boldsymbol{V}_3$, we introduce the matrix $\boldsymbol{M}_k$ defined in (C.2.3) as $\boldsymbol{M}_k := \mathbf{U}^\top\hat{\mathbf{U}}\mathbf{J}^{k+1}|\hat{\mathbf{S}}|^{-k-1/2} - |\mathbf{S}|^{-k-1/2}\mathbf{U}^\top\hat{\mathbf{U}}\mathbf{J}^{k+1}$. We decompose $\boldsymbol{M}_k$ following (C.2.3) as

$$\boldsymbol{M}_k = -\mathbf{H}_k\circ\left(\left(\mathbf{U}^\top\hat{\mathbf{U}}\hat{\mathbf{S}}-\mathbf{S}\mathbf{U}^\top\hat{\mathbf{U}}\right)\mathbf{J}^k + |\mathbf{S}|\left(\mathbf{J}\mathbf{U}^\top\hat{\mathbf{U}}-\mathbf{U}^\top\hat{\mathbf{U}}\mathbf{J}\right)\mathbf{J}^k\right),$$

where $\mathbf{H}_k$ is defined as (C.2.3). Notice that $\mathbf{U}^\top\hat{\mathbf{U}}\hat{\mathbf{S}}-\mathbf{S}\mathbf{U}^\top\hat{\mathbf{U}} = \mathbf{U}^\top(\widehat{\boldsymbol{D}}-\boldsymbol{D}^\star)\hat{\mathbf{U}}$, which gives us $\|\mathbf{U}^\top\hat{\mathbf{U}}\hat{\mathbf{S}}-\mathbf{S}\mathbf{U}^\top\hat{\mathbf{U}}\|_F = O_p(\|\widehat{\boldsymbol{D}}-\boldsymbol{D}^\star\|_F) = O_p(\frac{N}{\rho_N M^{1/2}})$. In addition, following equation (13) in (C.2.3), we have $\|\mathbf{J}\mathbf{U}^\top\hat{\mathbf{U}}-\mathbf{U}^\top\hat{\mathbf{U}}\mathbf{J}\|_F = O_p(\|\boldsymbol{U}_{(+)}^\top\widehat{\boldsymbol{U}}_{(-)})\|_F) = O_p(1/\sqrt{\rho_N^2 M})$. Given that the ranks of $\mathbf{U}^\top\hat{\mathbf{U}}\hat{\mathbf{S}}-\mathbf{S}\mathbf{U}^\top\hat{\mathbf{U}}$ and $\mathbf{J}\mathbf{U}^\top\hat{\mathbf{U}}-\mathbf{U}^\top\hat{\mathbf{U}}\mathbf{J}$ are bounded and the fact that

$\|A\|_F \asymp \|A\|_{op}$ when rank of A is bounded. Then following (C.2.3), we have

$$\begin{aligned}\|\boldsymbol{M}_k\|_F \asymp \|\boldsymbol{M}_k\|_{op} &= O_p\left(N^{-k-3/2} \times \left(\frac{N}{\rho_N M^{1/2}} + N \times 1/\sqrt{\rho_N^2 M}\right)\right) \\ &= O_p\left(\frac{N^{-k-1/2}}{\rho_N M^{1/2}}\right).\end{aligned}$$

Then we have

$$\begin{aligned}\|\boldsymbol{V}_3\|_F &\leq \|\mathbf{U}\mathbf{S}\boldsymbol{M}_0\|_F + \|\widehat{\boldsymbol{D}} - \boldsymbol{D}\|_F \, \|\mathbf{U}\mathbf{S}\boldsymbol{M}_1\|_F + o_p(\|\boldsymbol{R}_{V_1}\|_F) \\ &\leq O_p\left(N \frac{N^{-1/2}}{\rho_N M^{1/2}}\right) + O_p\left(\frac{N^2}{\rho_N M^{1/2}} \frac{N^{-3/2}}{\rho_N M^{1/2}}\right) \\ &= O_p\left(\frac{N^{1/2}}{\rho_N M^{1/2}}\right).\end{aligned}$$

The transformed latent positions $\widetilde{\boldsymbol{\Theta}} = \boldsymbol{U}\,|\boldsymbol{S}|^{1/2}\boldsymbol{J}$ are identifiable and estimated by $\widehat{\boldsymbol{\Theta}} = \widehat{\boldsymbol{U}}|\widehat{\boldsymbol{S}}|^{1/2}\boldsymbol{J}$, which indicates that $\boldsymbol{W} = \boldsymbol{I}$. According to Equation (A.14) and the above results,

$$\|\widehat{\boldsymbol{\Theta}} - \widetilde{\boldsymbol{\Theta}}\|_F = O_p\left(\left(\frac{N}{\rho_N^2 M}\right)^{1/2}\right).$$

Note that $\boldsymbol{\Theta} = \widetilde{\boldsymbol{\Theta}}\boldsymbol{R}$, where $\boldsymbol{R}$ is a hyperbolic rotation such that $\boldsymbol{R}\,\boldsymbol{J}\,\boldsymbol{R}^\top = \boldsymbol{J}$. Using the fact that $\|\boldsymbol{A}\,\boldsymbol{R}\|_F = \|\boldsymbol{A}\|_F$ if $\boldsymbol{R}\,\boldsymbol{J}\boldsymbol{R}^\top = \boldsymbol{J}$, we have

$$\frac{1}{N}\inf_{\boldsymbol{R}} \|\widehat{\boldsymbol{\Theta}}\boldsymbol{R} - \boldsymbol{\Theta}\|_F^2 = O_p\left(\frac{1}{\rho_N^2 M}\right) = O_p\left(\frac{\Delta_{N,2}}{\rho_N^2 \sqrt{|\mathcal{S}|}}\right),$$

where the infimum is over all hyperbolic rotation matrices $\boldsymbol{R}$.

B Computational Details

B.1 Manifold Gradient Descent

We first derive the Euclidean gradient of the population loss with respect to the latent position $\boldsymbol{\theta}_h$ with $h \in \mathcal{V}$. The population loss is defined by

$$\ell(\boldsymbol{\Lambda}) := -\sum_{k=2}^{K}\sum_{e\in\mathcal{E}_k} z_e \log \pi(\alpha_{|e|}, \boldsymbol{\Theta}_e) + (1 - z_e) \log(1 - \pi(\alpha_{|e|}, \boldsymbol{\Theta}_e)),$$

and its gradient with respect to the latent position $\boldsymbol{\theta}_h$ with $h \in \mathcal{V}$ is:

$$\begin{aligned}
\nabla_{\boldsymbol{\theta}_h} \pi(\alpha_{|e|}, \boldsymbol{\Theta}_e) &= \frac{-2\,\alpha_{|e|}\,\exp(g(\boldsymbol{\Theta}_e))}{(1+\exp(g(\boldsymbol{\Theta}_e))^2}\,\nabla_{\boldsymbol{\theta}_h}\; g(\boldsymbol{\Theta}_e) \\
&= -\pi(\alpha_{|e|}, \boldsymbol{\Theta}_e)\left(1 - \frac{\pi(\alpha_{|e|}, \boldsymbol{\Theta}_e)}{2\,\alpha_{|e|}}\right)\nabla_{\boldsymbol{\theta}_h}\; g(\boldsymbol{\Theta}_e) \\
\nabla_{\boldsymbol{\theta}_h}\; g(\boldsymbol{\Theta}_e) &= \nabla_{\boldsymbol{\theta}_h}\left(\frac{1}{|e|}\sum_{i\in e}\left(d_i^{(e)}(\boldsymbol{\Theta}_e)\right)^p\right)^{1/p} \\
&= \frac{1}{p}\left(\frac{1}{|e|}\sum_{i\in e}\left(d_i^{(e)}(\boldsymbol{\Theta}_e)\right)^p\right)^{(1-p)/p}\nabla_{\boldsymbol{\theta}_h}\;\left(\frac{1}{|e|}\sum_{i\in e}\left(d_i^{(e)}(\boldsymbol{\Theta}_e)\right)^p\right) \\
\nabla_{\boldsymbol{\theta}_h}\left(\sum_{i\in e}\left(d_i^{(e)}(\boldsymbol{\Theta}_e)\right)^p\right) &= \sum_{i\in e} p\,\left(d_i^{(e)}(\boldsymbol{\Theta}_e)\right)^{p-1}\nabla_{\boldsymbol{\theta}_h} d_i^{(e)}(\boldsymbol{\Theta}_e).
\end{aligned}$$

For $i \neq h$, $\nabla_{\boldsymbol{\theta}_h} d_i^{(e)}(\boldsymbol{\Theta}_e)$ is

$$\begin{aligned}
\nabla_{\boldsymbol{\theta}_h} d_i^{(e)}(\boldsymbol{\Theta}_e) &= \nabla_{\boldsymbol{\theta}_h}\left(\sum_{j\in e,\, j\neq i} d_{\mathcal{L}}(\boldsymbol{\theta}_i, \boldsymbol{\theta}_j)\right) \\
&= \nabla_{\boldsymbol{\theta}_h} d_{\mathcal{L}}(\boldsymbol{\theta}_i, \boldsymbol{\theta}_h),
\end{aligned}$$

while we get for $i = h$

$$\nabla_{\boldsymbol{\theta}_h} d_h^{(e)}(\boldsymbol{\Theta}_e) = \sum_{i\in e,\, i\neq h} \nabla_{\boldsymbol{\theta}_h} d_{\mathcal{L}}(\boldsymbol{\theta}_i, \boldsymbol{\theta}_h).$$

With $\boldsymbol{J} = \mathrm{diag}(-1, \mathbf{1}_r) \in \mathbb{R}^{r+1}$, $\mathbf{1}_n = (1, 1, \ldots) \in \mathbb{R}^n$ being a vector of n ones, and $\Delta_{i,h} = 1/(\langle \boldsymbol{\theta}_i, \boldsymbol{\theta}_h \rangle_{\mathcal{L}}^2 - 1)^{0.5}$, we have

$$\nabla_{\boldsymbol{\theta}_h} d_{\mathcal{L}}(\boldsymbol{\theta}_i, \boldsymbol{\theta}_h) = -\boldsymbol{J}\Delta_{i,h}\,\boldsymbol{\theta}_i. \tag{B.1}$$

Plugging Equation (B.1) into the previous equations gives for $i = h$

$$\nabla_{\boldsymbol{\theta}_h} d_h^{(e)}(\boldsymbol{\Theta}_e) = -\boldsymbol{J}\sum_{i\in e,\, i\neq h}\Delta_{i,h}\,\boldsymbol{\theta}_i$$

and for $i \neq h$

$$\nabla_{\boldsymbol{\theta}_h} d_i^{(e)}(\boldsymbol{\Theta}_e) = -\boldsymbol{J}\,\Delta_{i,h}\,\boldsymbol{\theta}_i.$$

This, in turn, allows us to calculate

$$\begin{aligned}
\nabla_{\boldsymbol{\theta}_h} \sum_{i \in e} \left(d_i^{(e)}(\boldsymbol{\Theta}_e) \right)^p &= -p\, \boldsymbol{J} \sum_{i \in e; i \neq h} \left(\left(d_i^{(e)}(\boldsymbol{\Theta}_e) \right)^{p-1} + \left(d_h^{(e)}(\boldsymbol{\Theta}_e) \right)^{p-1} \right) \Delta_{i,h}\, \boldsymbol{\theta}_i, \\
\nabla_{\boldsymbol{\theta}_h}\, g(\boldsymbol{\Theta}_e) &= \frac{-\boldsymbol{J}}{|e|} \left(\frac{1}{|e|} \sum_{i \in e} \left(d_i^{(e)}(\boldsymbol{\Theta}_e) \right)^p \right)^{(1-p)/p} \\
&\times \left(\sum_{i \in e; i \neq h} \left(\left(d_i^{(e)}(\boldsymbol{\Theta}_e) \right)^{p-1} + \left(d_h^{(e)}(\boldsymbol{\Theta}_e) \right)^{p-1} \right) \Delta_{i,h}\, \boldsymbol{\theta}_i \right),
\end{aligned}$$

and

$$\begin{aligned}
\nabla_{\boldsymbol{\theta}_h}\, \pi(\alpha_{|e|}, \boldsymbol{\Theta}_e) &= -\pi(\alpha_{|e|}, \boldsymbol{\Theta}_e) \left(1 - \frac{\pi(\alpha_{|e|}, \boldsymbol{\Theta}_e)}{2\, \alpha_{|e|}} \right) \frac{-\boldsymbol{J}}{|e|} \left(\frac{1}{|e|} \sum_{i \in e} \left(d_i^{(e)}(\boldsymbol{\Theta}_e) \right)^p \right)^{(1-p)/p} \\
&\times \left(\sum_{i \in e; i \neq h} \left(\left(d_i^{(e)}(\boldsymbol{\Theta}_e) \right)^{p-1} + \left(d_h^{(e)} \right)^{p-1} \right) \Delta_{i,h}\, \boldsymbol{\theta}_i \right).
\end{aligned}$$

Defining

$$\begin{aligned}
A_1(e, \Lambda) &= \left(\frac{1}{|e|} \sum_{i \in e} \left(d_i^{(e)}(\boldsymbol{\Theta}_e) \right)^p \right)^{(1-p)/p} \in \mathbb{R} \\
\boldsymbol{A}_2^h(e, \Lambda) &= \frac{\boldsymbol{J}}{|e|} \left(\sum_{i \in e; i \neq h} \left(\left(d_i^{(e)}(\boldsymbol{\Theta}_e) \right)^{p-1} + \left(d_h^{(e)} \right)^{p-1} \right) \Delta_{i,h}\, \boldsymbol{\theta}_i \right) \in \mathbb{R}^{r+1},
\end{aligned}$$

we can write

$$\nabla_{\boldsymbol{\theta}_h}\, \pi(\alpha_{|e|}, \boldsymbol{\Theta}_e) = \pi(\alpha_{|e|}, \boldsymbol{\Theta}_e) \left(1 - \frac{\pi(\alpha_{|e|}, \boldsymbol{\Theta}_e)}{2\, \alpha_{|e|}} \right) A_1(e, \Lambda)\, \boldsymbol{A}_2^h(e, \Lambda)$$

Finally, the derivative can be derived as follows

$$\begin{aligned}
\nabla_{\boldsymbol{\theta}_h}\, \ell(\boldsymbol{\Lambda}) &= -\sum_{k=2}^{K} \sum_{e \in \mathcal{E}_k} \mathbf{1}_{\{h \in e\}} \frac{z_e - \pi(\alpha_{|e|}, \boldsymbol{\Theta}_e)}{\pi(\alpha_{|e|}, \boldsymbol{\Theta}_e)\, (1 - \pi(\alpha_{|e|}, \boldsymbol{\Theta}_e))} \nabla_{\boldsymbol{\theta}_h}\, \pi(\alpha_{|e|}, \boldsymbol{\Theta}_e) \\
&= -\sum_{k=2}^{K} \sum_{e \in \mathcal{E}_k} \mathbf{1}_{\{h \in e\}} \frac{z_e - \pi(\alpha_{|e|}, \boldsymbol{\Theta}_e)}{1 - \pi(\alpha_{|e|}, \boldsymbol{\Theta}_e)} \left(1 - \frac{\pi(\alpha_{|e|}, \boldsymbol{\Theta}_e)}{2\, \alpha_{|e|}} \right) A_1(e, \Lambda)\, \boldsymbol{A}_2^h(e, \Lambda).
\end{aligned}$$

Note that we derived the population gradient, but letting $e \in \mathcal{S}_k \coloneqq \mathcal{S}_k^{(0)} \bigcup \mathcal{S}_k^{(1)}$ and including the reciprocal weight μ_e as a multiplicative constant yields the following sample gradient gradient:

$$\nabla_{\boldsymbol{\theta}_h}\, \widehat{\ell}(\boldsymbol{\Lambda}) = -\sum_{k=2}^{K} \sum_{e \in \mathcal{S}_k} \frac{\mathbf{1}_{\{h \in e\}}}{\mu_e} \frac{z_e - \pi(\alpha_{|e|}, \boldsymbol{\Theta}_e)}{1 - \pi(\alpha_{|e|}, \boldsymbol{\Theta}_e)} \left(1 - \frac{\pi(\alpha_{|e|}, \boldsymbol{\Theta}_e)}{2\, \alpha_{|e|}} \right) A_1(e, \Lambda)\, \boldsymbol{A}_2^h(e, \Lambda).$$

B.2 Estimation under Euclidean Geometry

In our experiments, we estimate the novel Latent Space Model for Hyperedges under the assumption that the latent positions $\boldsymbol{\Theta}$ are in either hyperbolic or Euclidean space. For the specification based on the Euclidean geometry, we employ the same type of maximization with the sole difference that the cyclical updates of $\boldsymbol{\theta}_h$ for all $h \in \mathcal{V}$ are carried out by the Euclidean variant of the manifold gradient descent algorithm, which reduces Equation (2) to the gradient descent updates:

$$\boldsymbol{\theta}_h^{(t+1)} \;=\; \boldsymbol{\theta}_h^{(t)} - \eta_h^{(t+1)} \nabla_{\boldsymbol{\theta}_h} \widehat{\ell}_{\mathcal{E}}(\boldsymbol{\Lambda}), \tag{B.2}$$

where $\eta_h^{(t+1)}$ is a learning rate that is set by Brent's method to minimize the negative likelihood and $\nabla_{\boldsymbol{\theta}_h} \widehat{\ell}_{\mathcal{E}}(\boldsymbol{\Lambda})$ denotes the gradient of the sample likelihood with $\boldsymbol{\Theta}$ being in the Euclidean space.

Contrasting the definition in Equation (1), the function $d_i^{(e)}(\boldsymbol{\Theta}_e)$ is substitute by its Euclidean analog:

$$d_{\mathcal{E},i}^{(e)}(\boldsymbol{\Theta}_e) \;\coloneqq\; \sum_{h \in e \setminus \{i\}} d_{\mathcal{E}}(\boldsymbol{\theta}_i, \boldsymbol{\theta}_h),$$

with

$$d_{\mathcal{E}}(\boldsymbol{\theta}_i, \boldsymbol{\theta}_h) \;\coloneqq\; \|\boldsymbol{\theta}_i - \boldsymbol{\theta}_h\|_2.$$

To obtain $\nabla_{\boldsymbol{\theta}_h} \widehat{\ell}_{\mathcal{E}}(\boldsymbol{\Lambda})$, we substitute the derivative of the hyperbolic distance between $\boldsymbol{\theta}_i$ and $\boldsymbol{\theta}_h$ with respect to $\boldsymbol{\theta}_h$ with the partial derivative of the Euclidean distance:

$$\nabla_{\boldsymbol{\theta}_h} d_{\mathcal{E}}(\boldsymbol{\theta}_i, \boldsymbol{\theta}_h) \;=\; -\frac{\boldsymbol{\theta}_i - \boldsymbol{\theta}_h}{\|\boldsymbol{\theta}_i - \boldsymbol{\theta}_h\|_2}.$$

Defining

$$\begin{aligned}
B_1(e, \Lambda) \;&=\; \left(\frac{1}{|e|} \sum_{i \in e} \left(d_{\mathcal{E},i}^{(e)}(\boldsymbol{\Theta}_e) \right)^p \right)^{(1-p)/p} \in \mathbb{R} \\
\boldsymbol{B}_2^h(e, \Lambda) \;&=\; \frac{1}{|e|} \left(\sum_{i \in e; i \neq h} \left(\left(d_{\mathcal{E},i}^{(e)}(\boldsymbol{\Theta}_e) \right)^{p-1} + \left(d_{\mathcal{E},h}^{(e)}(\boldsymbol{\Theta}_e) \right)^{p-1} \right) \frac{\boldsymbol{\theta}_i - \boldsymbol{\theta}_h}{\|\boldsymbol{\theta}_i - \boldsymbol{\theta}_h\|_2} \right) \in \mathbb{R}^{r+1},
\end{aligned}$$

we can write

$$\nabla_{\boldsymbol{\theta}_h} \pi(\alpha_{|e|}, \boldsymbol{\Theta}_e) \;=\; \pi(\alpha_{|e|}, \boldsymbol{\Theta}_e) \left(1 - \frac{\pi(\alpha_{|e|}, \boldsymbol{\Theta}_e)}{2\,\alpha_{|e|}}\right) B_1(e, \Lambda)\, \boldsymbol{B}_2^h(e, \Lambda)$$

Then the the derivative of the population loss is

$$\nabla_{\boldsymbol{\theta}_h} \ell_{\mathcal{E}}(\boldsymbol{\Lambda}) \;=\; -\sum_{k=2}^{K} \sum_{e \in \mathcal{E}_k} \mathbf{1}_{\{h \in e\}} \frac{z_e - \pi(\alpha_{|e|}, \boldsymbol{\Theta}_e)}{1 - \pi(\alpha_{|e|}, \boldsymbol{\Theta}_e)} \left(1 - \frac{\pi(\alpha_{|e|}, \boldsymbol{\Theta}_e)}{2\,\alpha_{|e|}}\right) B_1(e, \Lambda)\, \boldsymbol{B}_2^h(e, \Lambda).$$

The respective gradient of the sample loss is then:

$$\nabla_{\boldsymbol{\theta}_h} \widehat{\ell}_{\mathcal{E}}(\boldsymbol{\Lambda}) \;=\; -\sum_{k=2}^{K} \sum_{e \in \mathcal{S}_k} \frac{\mathbf{1}_{\{h \in e\}}}{\mu_e} \frac{z_e - \pi(\alpha_{|e|}, \boldsymbol{\Theta}_e)}{1 - \pi(\alpha_{|e|}, \boldsymbol{\Theta}_e)} \left(1 - \frac{\pi(\alpha_{|e|}, \boldsymbol{\Theta}_e)}{2\,\alpha_{|e|}}\right) B_1(e, \Lambda)\, \boldsymbol{B}_2^h(e, \Lambda).$$

Given this partial derivative, we can carry out update rule Equation (B.2).

B.3 Initialization

Sparsity parameters Our implementation first updates the sparsity parameters and then the positions. Therefore, no initial values for the sparsity parameters are needed.

Positions Following Nickel and Kiela (2017, 2018), we initialize all positions uniformly around the origin $(0, 0)$ of the Poincaré disk. For all reported experiments, we sample the positions uniformly from a square with length 0.2. These initial positions are transformed to the Lorentz model by the function

$$f^{-1}(\boldsymbol{\theta}) \;=\; \left(1 + \|\boldsymbol{\theta}\|_2^2, \frac{2\,\boldsymbol{\theta}}{1 - \|\boldsymbol{\theta}\|_2^2}\right), \tag{B.3}$$

which is the inverse of the bijective function f from Section 2 of the main article.

C Simulating Positions

We generate the positions for N units on the Poincaré disk by their polar coordinates. For simplicity, we detail the procedure with $r = 2$. Polar coordinates are a way to represent

each point $(x, y) \in \mathcal{P}^2$ in terms of the radial coordinate $x_\rho \in [0, 1)$, which is its Euclidean distance to the point $(0, 0)$, and the angular coordinate $y_\theta \in [0, 2\pi)$, which is the angle between the straight line from (x, y) to $(0, 0)$ and the horizontal axis.

The generated positions are controlled by parameters $\gamma > 0$ and $\rho \in (0, 1]$:

1. Generate the radial coordinates $Z_1, \ldots, Z_N \overset{\text{iid}}{\sim} \mathrm{Z}(\gamma, \rho)$ with density at $z \in [0, \rho]$

$$f_Z(z \mid \gamma, \rho) \;\; = \;\; \gamma \frac{\sinh(\gamma\, z)}{\cosh(\rho\, \gamma) - 1},$$

   which closely approximates an exponential distribution with rate γ, truncated at ρ.

2. Generate the angular coordinates $S_1, \ldots, S_N \overset{\text{iid}}{\sim} \text{Uniform}[0,\, 2\,\pi]$.

3. Transform the polar coordinates to the Cartesian coordinates: for ith position we get $(z_i \cos(s_i),\; z_i \sin(s_i))$.

For all experiments, we set $\gamma = 3$ and $\rho = 1/2$.

D Application to Newswire Data

D.1 Data

We apply our proposed method to the Newswire data set (Silcock et al., 2014) containing approximately 2.7 million articles in the public domain. Using a topic classification based on a neural network architecture, these articles were tagged by with entities, i.e., people, that are mentioned in them and topic of the article. For this application, we focused on articles with one of the following topics: "Civil Rights", "Defense", "Federal Government Operations", "Macroeconomics", "International Affairs", "Labor, Immigration, and Employment". These entities correspond to the units defined in the manuscript. Silcock et al. (2014) provided the Wikidata ID for all units. This information allows us to link each entity to the database Wikidata. Wikidata is an open-source database feeding into Wikipedia

articles, from which we derived each unit's birthday and political party affiliation. Silcock et al. (2014) supplement these data by providing the profession for each unit. As stated in the main manuscript, our analysis focuses on hyperedges of sizes 2, 3, and 4. The inclusion criteria for units are as follows:

1. Profession: The profession of the unit is "politician", "judge", "lawyer", "military officer", or "military personnel".

2. Birth: The birthday of the unit is before the 1st of January, 1900.

3. Political affiliation: The unit was registered as a Democrat or Republican (or both) in the U.S.

4. Activity: The unit was mentioned in at least five articles with other units that also fulfill all inclusion criteria for hyperedges of sizes $k \in \{2, 3, 4\}$.

Because the final criterion is now evaluated only with respect to hyperedges of sizes $k \in 2, 3, 4$, the total counts of realized hyperedges differ slightly from the reported values in Section 7.2: $|\mathcal{E}_2^{(1)}| = 4{,}537$, $|\mathcal{E}_3^{(1)}| = 2{,}761$, $|\mathcal{E}_4^{(1)}| = 1{,}148$.

D.2 Additional Results of Euclidean and Hyperbolic Model

Estimates of Θ The correlation between the pairwise distances implied by the hyperbolic and Euclidean latent models is moderate, .448, with hyperbolic distances being on average .738 longer than the corresponding Euclidean distances. In Figure 8, we present two-dimensional kernel density estimates of the pairwise distances between all units under the hyperbolic and Euclidean latent space models. For points $\boldsymbol{x}, \boldsymbol{y} \in \mathcal{L}^2$, the hyperbolic distance is defined as $\operatorname{arcosh}(-\langle \boldsymbol{x}, \boldsymbol{y} \rangle_{\mathcal{L}})$, where $\langle \cdot, \cdot \rangle_{\mathcal{L}}$ denotes the Lorentzian inner product defined in Section 2. The Euclidean distance between $\boldsymbol{x}, \boldsymbol{y} \in \mathbb{R}^2$ is $\|\boldsymbol{x} - \boldsymbol{y}\|_2$. Figure 8 reveals a positive

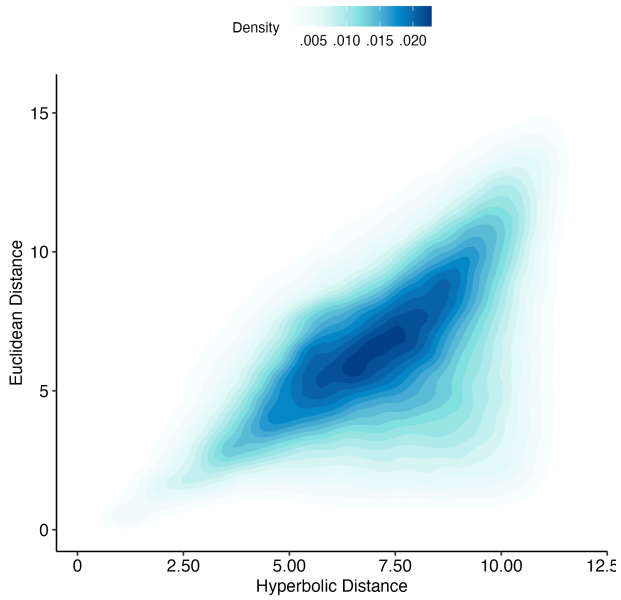

Figure 8: Two-dimensional kernel density estimator of the differences in pairwise distances according to the model under Euclidean and hyperbolic geometries and the minimal distance to the center within pair.

association between the two distance measures, while also highlighting discrepancies that suggest each geometry captures different structural aspects of the hypergraph.

Turning to the question of which node pairs exhibit the largest discrepancies in distance under the two geometries, we investigate whether these differences are particularly pronounced for pairs involving units near the center (minimal distance to center within pair is small) or periphery of the Poincaré disk(minimal distance to center within pair is large). Figure 9 reveals that pairs for which at least one node lies close to the center tend to have substantially larger distances in the hyperbolic model compared to the Euclidean model. Euclidean space compresses the center, thus underestimates distances between central units. In contrast, for pairs where both units are located farther from the center, the distances derived from both geometries more comparable.

To facilitate a more direct comparison between the estimated positions under hyperbolic and Euclidean geometries, we project the positions obtained in hyperbolic space into

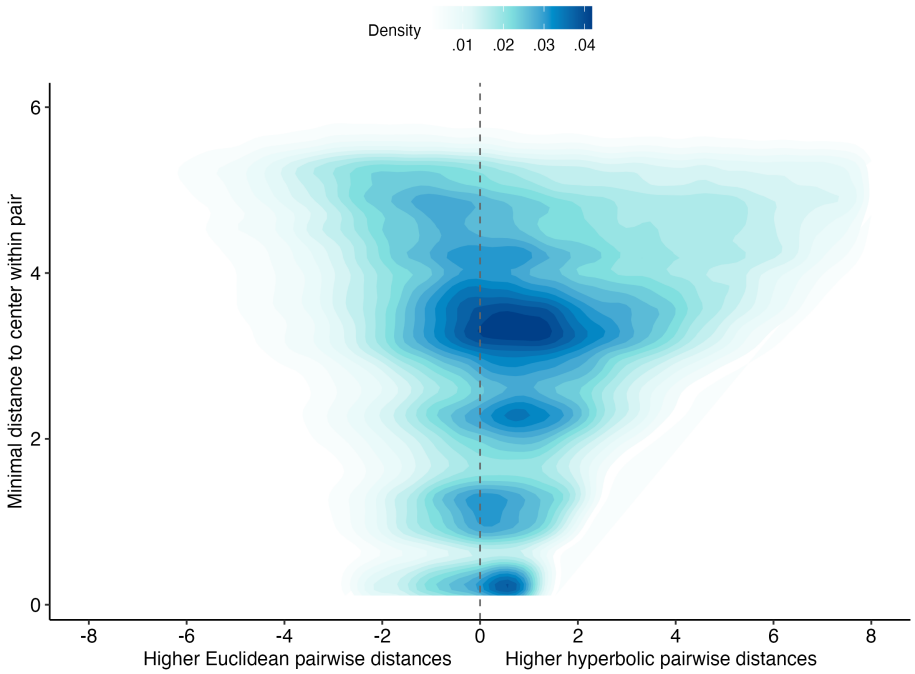

Figure 9: Two-dimensional kernel density estimator of the pairwise distances between all units according to the model under Euclidean and hyperbolic geometries.

Euclidean space with the following procedure:

1. Compute all pairwise hyperbolic distances between the positions of all N units.

2. Apply multidimensional scaling to distance matrix to obtain a configuration in Euclidean space to approximately preserve the hyperbolic distances (Cox and Cox, 2000).

3. Use Procrustes analysis to align the resulting configuration with the Euclidean positions, maximizing structural similarity (Young and Householder, 1938).

We refer to the hyperbolic positions obtained through this transformation as transformed hyperbolic positions.

Figure 10 (a) displays these transformed positions, while Figure 10 (b) shows the original Euclidean estimates. Both position clouds appear visually distinct, demonstrating that positions in hyperbolic space capture different latent similarities than those in Euclidean space. The hyperbolic configuration reveals a peripheral clustering pattern. In contrast, the

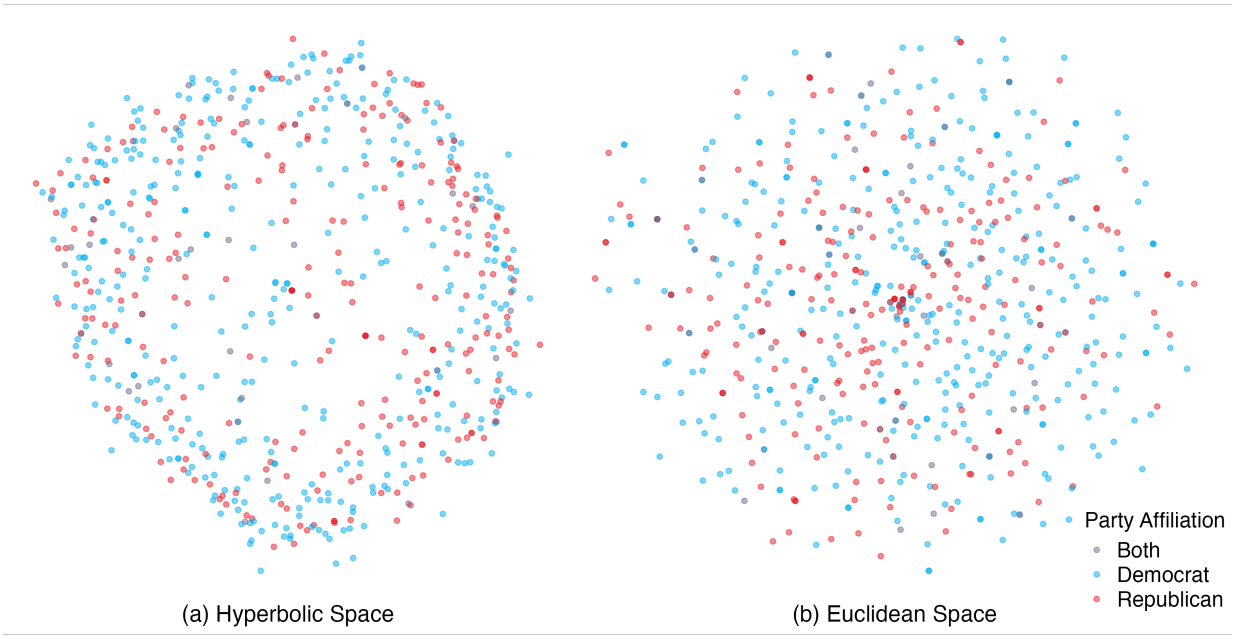

(a) Hyperbolic Space (b) Euclidean Space

Figure 10: Estimated latent positions obtained by fitting the model under hyperbolic and Euclidean geometry. The transformed hyperbolic space positions are shown in (a), while the original positions from the model under Euclidean space are shown in (b).

Euclidean positions appear more compact and contracted around their centroid. Compared to Figure 4 (a) in the main text, the transformed positions appear contracted toward the center of the space, as expected given that hyperbolic distances to the origin are shorter than their Euclidean counterparts.

Estimates of α Figure 11 (a) shows the estimates of α_2, α_3, and α_4 based on the hyperbolic and Euclidean space models. In line with expectations, we find that $\widehat{\alpha}_2 > \widehat{\alpha}_3 > \widehat{\alpha}_4$, suggesting that the density of smaller hyperedges is higher than the density of larger hyperedges. This observation holds irrespective of the geometry of the space. The estimates converge within the first 100 iterations for both geometries.

Approximate negative loglikelihood Figure 11 (b) displays the trace of the approximate negative loglikelihood across 100 iterations. Convergence appears to be achieved

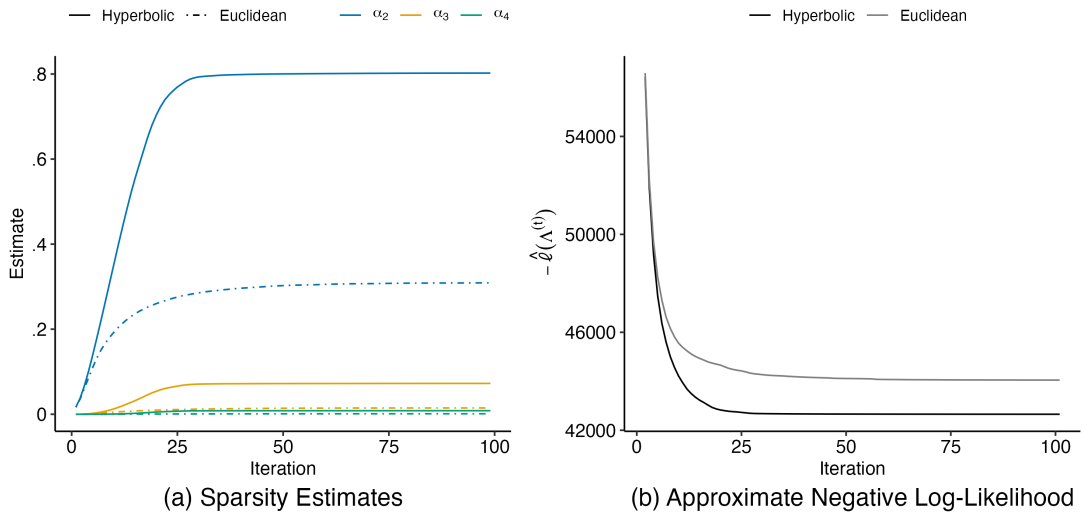

Figure 11: (a) Trace plot of sparsity parameter estimates (blue for $\hat{\alpha}_2$, yellow for $\hat{\alpha}_3$, and green for $\hat{\alpha}_4$) of the Latent Space Model based on hyperbolic (—, solid line) and Euclidean geometry (-·-, dotdashed line). (b) Trace plot of approximate loglikelihood of the Latent Space Model based on hyperbolic (black) and Euclidean geometry (black).

under both geometries after approximately 50 iterations. However, we observe that the hyperbolic geometry is able to achieve a lower value of the approximate loss function than the Euclidean geometry.

D.3 Sensitivity Analyses

Choice of p As mentioned in the manuscript, we fix $p \in \mathbb{R}$. To assess the sensitivity of the results to the choice of p, we estimate the hyperbolic latent space model with $p \in \{-25, -20\}$. We assess the sensitivity of the results to changes of p in two ways. First, in Figure 12 we conduct out-of-sample predictions as described in Section 6.2 of the manuscript. Second, we compare the estimates of the sparsity parameters under $p = -25$ and $p = -20$. Figure 13 suggests that the results are not too sensitive to the choice of p, as long as $p < 20$.

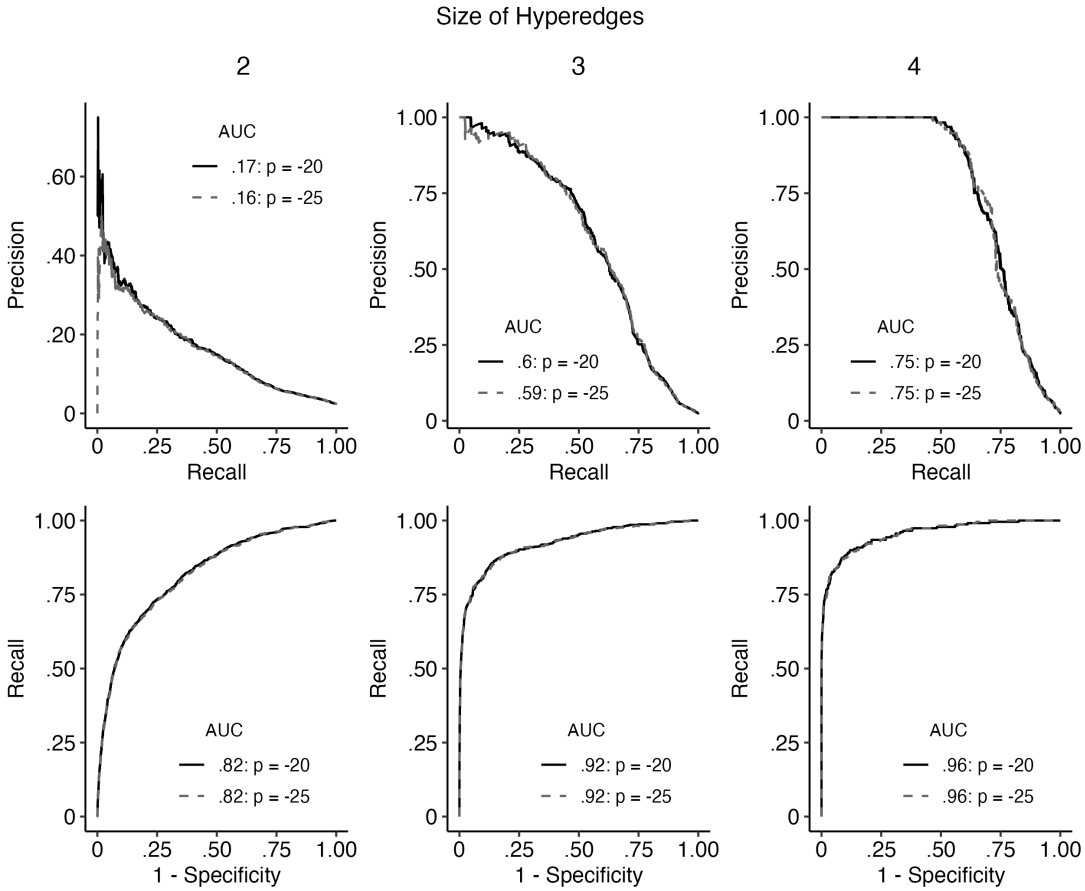

Figure 12: Newswire data: Receiver-Operator Characteristic (ROC) and Precision-Recall (PR) curve of out-of-sample predictions of hyperedges, based on hyperbolic geometry with $p \in \{-25, -20\}$.

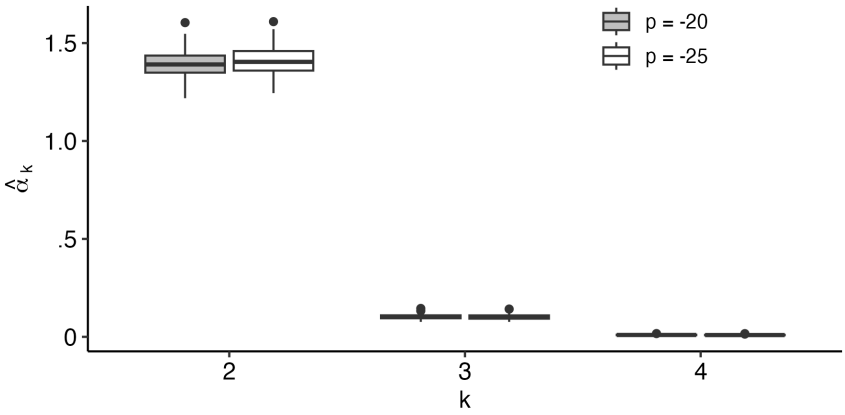

Figure 13: Boxplots of sparsity parameter estimates $\widehat{\alpha}_2$, $\widehat{\alpha}_3$, $\widehat{\alpha}_4$ based on the latent space model under hyperbolic geometry with $p \in \{-25, -20\}$.

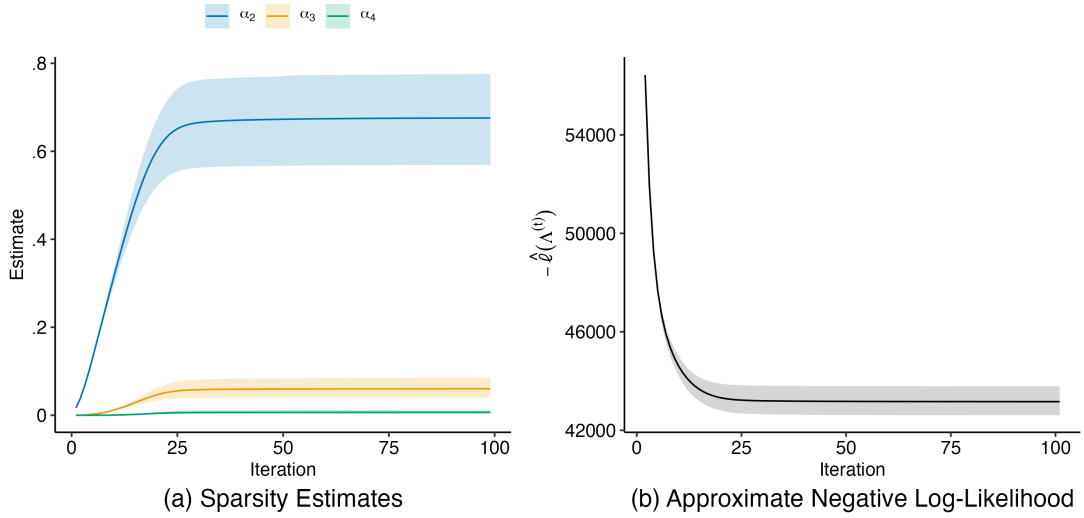

Figure 14: Results based on different initializations and sampled control hyperedges: (a) Range of trace plots of sparsity parameter estimates (blue for $\hat{\alpha}_2$, yellow for $\hat{\alpha}_3$, and green for $\hat{\alpha}_4$) based on the Latent Space Model based on hyperbolic geometry. (b) Approximate loglikelihood per iteration, where the solid line represents the point-wise average loglikelihoods.

Initial positions and sampled controls In the main manuscript, we initialize the positions of units using 100 different initial positions but fix the sampled control hyperedges used to effectively approximate the full likelihood as detailed in Section 4.2. In this robust-

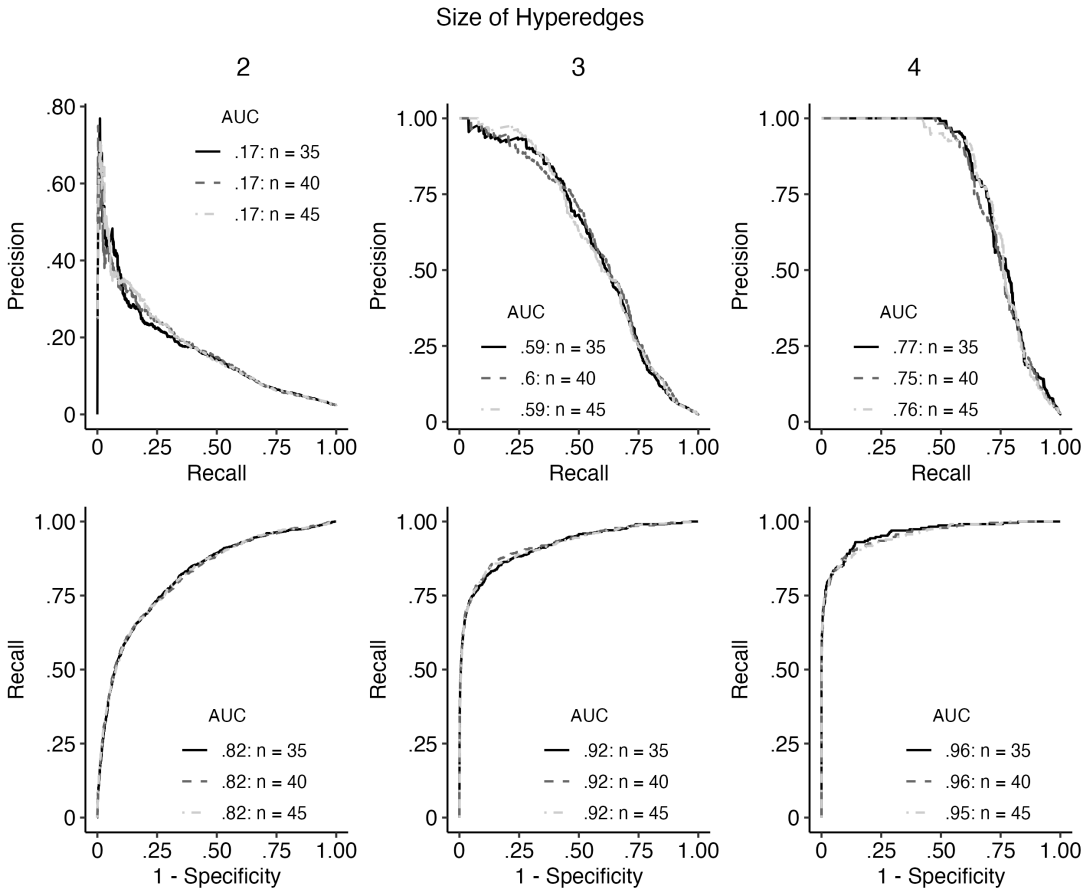

Figure 15: Newswire data: Receiver-Operator Characteristic (ROC) and Precision-Recall (PR) curve of out-of-sample predictions of hyperedges, based on embedding units in hyperbolic space with $n \in \{35, 40, 45\}$.

ness check, we randomize the starting positions but also the sampled controls. First, we see in Figure 14 (a) that the loglikelihood of the model converges after a reasonable time regardless of initial value. Second, the range of traceplots in Figure 14 (b) suggest that the sparsity parameter estimates do not vary substantially between runs and the algorithm does not seem to be trapped in local minima. In summary, both plots show evidence of the robustness of our algorithm to different initializations and sampled controls.

Different number of control samples We repeated the analysis using an increased number of samples per realized hyperedge. Figure 15 reports the out-of-sample perfor-

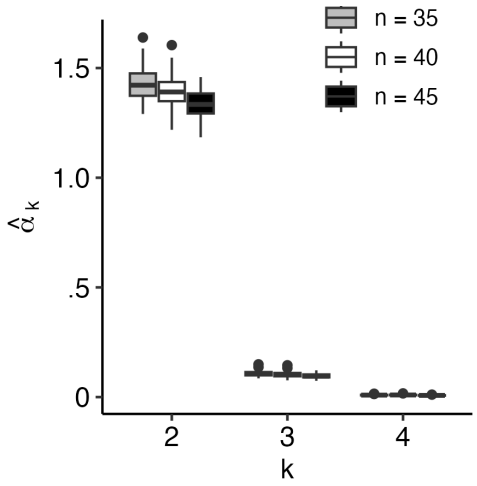

Figure 16: Boxplots of sparsity parameter estimates $\widehat{\alpha}_2$, $\widehat{\alpha}_3$, $\widehat{\alpha}_4$ based on the latent space model under hyperbolic geometry with $n \in \{35, 40, 45\}$.

mance for $n \in \{35, 40, 45\}$. Figure 16 displays the estimated sparsity parameters under all three settings. The results indicate that performance remains stable under moderate perturbations of n.

E Computational Settings

The proposed models and methods are implemented in the `R` package `hyperspace`, which is provided as part of the replication package. Most routines of this package are implemented in `C++` and imported to `R` using the `R` package `Rcpp` (Eddelbuettel and François, 2011). The experiments were carried out on a server running `R` version 4.4.1 under Red Hat Enterprise Linux 8.10. We used 100 cores and approximately 60 GB of RAM.

Supplementary Material References

Cox, T. and M. Cox (2000). *Multidimensional Scaling*. Boca Raton: Chapman & Hall/CRC.

Eddelbuettel, D. and R. François (2011). Rcpp: Seamless R and C++ integration. *Journal of Statistical Software 40*(8), 1–18.

Rubin-Delanchy, P., J. Cape, M. Tang, and C. E. Priebe (2022). A statistical interpretation of spectral embedding: the generalised random dot product graph. *Journal of the Royal Statistical Society Series B: Statistical Methodology 84*, 1446–1473.

Sen, B. (2018). A gentle introduction to empirical process theory and applications. *Lecture Notes, Columbia University*, 28–29. http://www.stat.columbia.edu/ bodhi/Talks/Emp-Proc-Lecture-Notes.pdf.

Silcock, E., A. Arora, L. D'Amico-Wong, and M. Dell (2014). Newswire: A large-scale structured database of a century of historical news. In *Advances in Neural Information Processing Systems*, pp. 1–12.

Tabaghi, P. and I. Dokmanić (2020). Hyperbolic distance matrices. In *ACM SIGKDD International Conference on Knowledge Discovery & Data Mining*, pp. 1728–1738.

Tang, M. and C. E. Priebe (2018). Limit theorems for eigenvectors of the normalized Laplacian for random graphs. *The Annals of Statistics 46*(5), 2360–2415.

Young, G. and A. S. Householder (1938). Discussion of a set of points in terms of their mutual distances. *Psychometrika 3*(1), 19–22.